Current Titles

National Center for Electron Microscopy

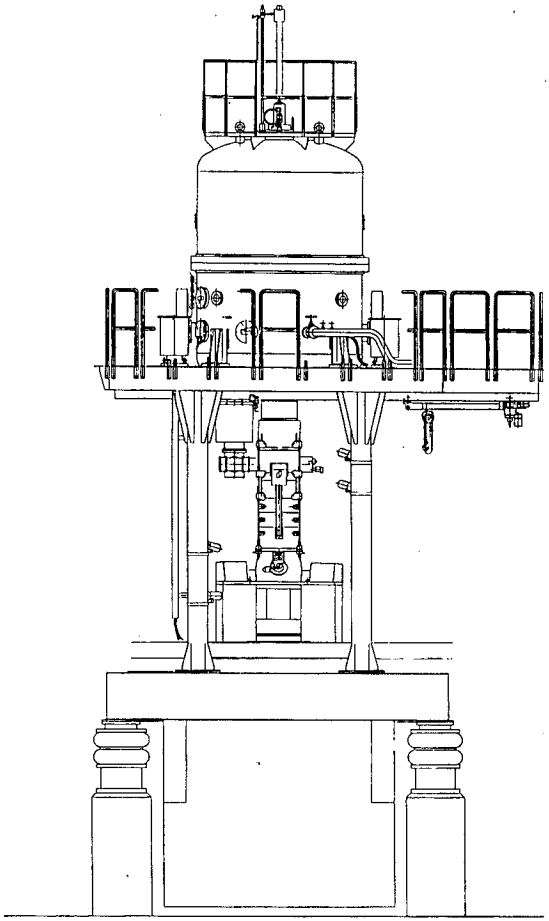

April 1996

DISCLAIMER

DISCLAIMER

Please send a reprint of the paper(s):

Number	First Author	Title (first two words)

Name_____ Date _____

Affiliation _____

Address _____

_____

Please send a reprint of the paper(s):

Number	First Author	Title (first two words)

Name_____ Date _____

Affiliation _____

Address _____

_____

National Center for Electron Microscopy
Berkeley Lab
MS 72
Berkeley, CA 94720
U.S.A.

National Center for Electron Microscopy
Berkeley Lab
MS 72
Berkeley, CA 94720
U.S.A.

Current Titles

National Center for Electron Microscopy
Ernest Orlando Lawrence
Berkeley National Laboratory
University of California
Berkeley, California 94720

April 1996

For current information about the NCEM
see our www page at

http://ncem.lbl.gov/ncem.html

The NCEM is supported by the Director, Office of Energy Research, Office of Basic Energy Sciences, Materials Sciences Division of the U.S. Department of Energy under Contract No. DE-AC03-76SF00098.

PUB-719

This booklet is published for those interested in current research being conducted at the National Center for Electron Microscopy. Copies of available papers may be ordered using the enclosed reprint request cards.

Articles are listed alphabetically by journal.
Conference proceedings follow journals.

The NCEM is a DOE-designated national user facility and is available at no charge to qualified researchers. Access is controlled by an external steering committee. For a user's guide or other information, please contact Gretchen Hermes:

by mail: National Center for Electron Microscopy
Berkeley Lab
MS 72
Berkeley, California 94720
U.S.A.

by phone: 510-486-5006

by fax: 510-486-5888

by e-mail: GHermes@lbl.gov

or find us on the world wide web at
http://ncem.lbl.gov/ncem.html

Pub 475 ■ **NCEM User's Guide**

edited by J. Turner

NCEM User's Guide *1993*

User's guide to the National Center for Electron Microscopy, Lawrence Berkeley Laboratory, University of California, Berkeley.

Pub 658 ■ **NCEMSS Manual**

M.A. O'Keefe and R. Kilaas

NCEMSS Manual *1994*

Manual for the National Center for Electron Microscopy Simulation System for the simulation of HRTEM images.

36192 ■ Microstructure of Silicon Nitride Ceramics Sintered with Rare-Earth Oxides

Y. Goto and G. Thomas

Acta Met. et Mat. 43 923 *1995*

Microstructures of Si_3N_4 with crystallized grain boundaries of rare-earth silicates were investigated. β-Si_3N_4 grains in samples sintered with Yb_2O_3 were more elongated than those sintered with Dy_2O_3. Amorphous thin layers between crystallized grain boundaries of silicate and Si_3N_4 grains were recognized for both specimens sintered with Dy_2O_3 and with Yb_2O_3. In the sample sintered with Dy_2O_3, very clean grain boundaries between Si_3N_4 grains which did not contain the heavy elements were frequently recognized, while samples with Yb_2O_3 had an amorphous grain boundary phase containing Yb. Unusual structures with distorted lattice images in regions rich in Si and O were discovered in crystalline Dy-silicate phases.

37029 ■ Enhanced Saturation Magnetization, Electronic Structure and Compositional Segregation in Epitaxially Grown Co-Cr Thin Films

K.M. Krishnan

Appl. Phys. Lett. 67 2238-40 *1995*

We have used the recently established linear correlation between the total intensities of the $L_{3,2}$ "white lines" in electron energy-loss spectroscopy and the number of unoccupied 3d states to probe the local electronic structure in epitaxially grown Co-Cr thin films. The significant enhancement of saturation magnetization measured for these epitaxial films, when compared to homogenized bulk alloys, has been correlated directly to the unoccupied 3d states local to the Co atoms in these materials. These measurements are the first direct electronic structure evidence that may support models associating the enhancement of saturation magnetization with intragranular segregation in Co-Cr thin films.

36236 ■ **Growth and Characterization of ($Y_3Fe_5O_{12}$-$Bi_3Fe_5O_{12}$) Heterostructures by Pulsed Laser Deposition**

B.M. Simion, G. Thomas, R. Ramesh, V.G. Keramidas and R.L. Pfeffer

Appl. Phys. Lett. 66 830 *1995*

Superlattice heterostructures consisting of alternating single crystalline ferrimagnetic yttrium-iron-garnet (YIG) and bismuth-iron-garnet (BIG) thin film layers on gadolinium-gallium-garnet substances show an increased saturation magnetization with respect to that of the monolayered structures grown under the same conditions. The observed effect is attributed to the distortions introduced in the YIG layers by the adjacent BIG layers. In this letter, we report our growth approach, by pulsed laser deposition, of these unusually performing thin films heterostructures.

37184 ■ **Synthesis of GaN by N Ion Implantation in GaAs (001)**

X.W. Lin, M. Behar, R. Maltez, W. Swider, Z. Liliental-Weber and J. Washburn

Appl. Phys. Lett. 67 2699 *1995*

Both the hexagonal and cubic GaN phases were synthesized in GaAs (001) by 50 keV N ion implantation at 380°C and subsequent furnace annealing at 850-950°C for 10 min-2 h. For a fluence of 1.5×10^{17} cm^{-2}, transmission electron microscopy revealed that cubic GaN epitaxially crystallizes as precipitates in the GaAs matrix. A cubic-to-hexagonal GaN phase transition was observed for extended thermal anneals. By increasing the N fluence to 3×10^{17} cm^{-2}, a continuous buried layer of randomly oriented hexagonal-GaN nanocrystals was produced.

37000 ■ Rapid Thermal Annealing of LT-GaAs Layers at High Temperatures

Z. Liliental-Weber, X.W. Lin, J. Washburn and W. Schaff

Appl. Phys. Lett. 66 2086 *1995*

Rapid thermal annealing (750-950°C) of MBE-GaAs layers grown at low temperature (200°C) results in coarsening of As precipitates and transition from the crystalline to the amorphous phase. For the annealing at 850°C and higher ordering of these precipitates along the growth axes is taking place and the majority of precipitates have similar size. From the observed Ostwald ripening kinetics an activation energy consistent with the migration enthalpy of gallium vacancies (V_{Ga}) was determined confirming the presence of a high density of these defects in LT-GaAs layers. This experiment showed that diffusion of As_{Ga} antisite defects in the process of coarsening of As precipitates is assisted by V_{Ga} present due to the nonstoichiometric composition of the compound.

38101 ■ Nucleation and Evolution of Misfit Dislocations in ZnSe/GaAs(001) Heterostructures Grown by Low-Pressure Organometallic Vapor Phase Epitaxy

S. Ruvimov, E. Bourret, J. Washburn and Z. Liliental-Weber

Appl. Phys. Lett. 68 1 *1996*

Transmission electron microscopy and x-ray diffraction were used to study strain relaxation and the evolution of the dislocation structure in ZnSe epilayers grown by low-pressure organometallic vapor phase epitaxy on a (001) surface of semi-insulating GaAs. Before the ZnSe growth, the substrate surface was exposed to a flow of tertiarybutylarsine to promote an As-terminated surface. This surface treatment results in a low density of stacking faults; 60° misfit dislocations were observed at a layer thickness as low as 0.05 μm. This agrees well with the theoretical critical value for misfit dislocation formation in the ZnSe/GaAs system, but is much lower than experimental critical thicknesses reported earlier. Various mechanisms of misfit dislocation generation were observed at different growth stages. The evolution of the dislocation structure is discussed in relation with the morphology of the ZnSe layers.

no # ■ **Trace Oxygen Effects on Nanocrystalline Copper**

D.L. Olynick, J.M. Gibson and R.S. Averback

Appl. Phys. Lett. 68 343-345 *1996*

Using an ultra-high vacuum (UHV) magnetron sputtering system connected directly to a UHV transmission electron microscope (TEM), we study, in-situ, the effect of trace levels of oxygen contamination on the early stages of sintering, coalescence, and morphology. Whereas, nano-particles produced under clean conditions experience substantial sintering and grain growth upon contact, even at room temperature, particles deliberately exposed to trace amounts of oxygen remain distinct. It therefore appears difficult to form ultra-clean nanophase materials, at least for copper, due to rapid sintering. These systematic studies of particle morphology as a function of oxygen exposure shed light on nano-particle growth mechanisms in the gas phase and thus ways to approach the ideal nanophase material.

36610 ■ **Nucleation of Misfit Dislocations in $In_{0.2}Ga_{0.8}$ As Epilayers Grown on GaAs Substrates**

Y. Chen, Z. Liliental-Weber, J. Washburn, J.F. Klem and J.Y. Tsao

Appl. Phys. Lett. B 66 499 *1995*

Misfit dislocation arrays in $In_{0.2}Ga_{0.8}As$ epilayers grown on GaAs substrates tilted 2°-10° away from exact (001) toward varied directions have been studied by transmission electron microscopy. A method has been developed to determine the glide plane and the Burgers vector of each misfit dislocation in the tilted InGaAs/GaAs interfaces. Based on experimental observations and theoretical analyses, it is proposed that a stacking fault surrounded by a 30° partial is at first generated by a growth error, followed by thermally activated nucleation of a 90° partial dislocation that removes the stacking fault and forms a 60° dislocation. From the frequency of nucleation events versus the dislocation glide force, the energy barrier for dislocation nucleation of α and β 90° partial dislocations was determined to be equal to 1.5 and 1.4 eV respectively.

37885 **Quasi-one-dimensional CaF_2 Islands Formed on Si(001) by Molecular Beam Epitaxy**

D. Loretto, F.M. Ross and C.A. Lucas

Appl. Phys. Lett. *(in press)*

Quasi-one-diminsional CaF_2 islands, 5-10 nm in both width and height and several μm in length, have been grown on Si(001) by molecular beam epitaxy. Using conventional and high resolution transmission electron microscopy, we show that the islands grow in two symmetry-equivalent orientations and are bounded by {111} facets. The unusual island morphology is attributed to a low density of nucleation sites, the small lattice mismatch and the anisotropic CaF_2 surface energy.

38375 ■ **Recrystallization of High Energy As-implanted GaAs Studied by Transmission Electron Microscopy**

J. Jasinski, Y. Chen, J. Washburn, Z. Liliental-Weber, H.H. Tan, C. Jagadish and M. Kaminska

Appl. Phys. Lett. *(in press)* 68 1

Ion implantation damage and the regrowth process during thermal annealing of 2 MeV As-ion-implanted GaAs were studied by transmission electron microscopy. With low-temperature annealing, a high density of stacking faults was formed during the recrystallization process, but they were rarely observed with high-temperature annealing. At intermediate temperatures, a much lower density of stacking faults was generated at the upper interface between the buried amorphous layer and the crystal than that at the lower interface, where a higher concentration of As-implanted arsenic exists. Based on the observed experimental results, an atomic model is proposed to explain the formation of stacking faults induced by As clusters.

36462 ■ Solid-State Reaction in Pd/ZnSe Thin Film Contacts

K.J. Duxstad, E.E. Haller, J. Washburn, K.M. Yu, E.D. Bourret, J.M. Walker and X.W. Lin

Appl. Phys. Lett. *(submitted)*

We report on solid-state reactions in Pd thin film contacts on ZnSe at temperatures below 500° C. We found that a solid-state reaction was initiated at the Pd/ZnSe interface by annealing at 200° C. A tetragonal ternary phase, Pd_5ZnSe, consisting of highly oriented grains was formed as a result of this reaction. This phase was found to be stable up to an annealing temperature of 400° C. The crystallography and morphology of this ternary Pd-ZnSe phase was studied by x-ray diffraction and transmission electron microscopy; it has similarities to the analogous ternary Pd-GaAs phase formed in the Pd/GaAs contact structure. The Pd/ZnSe interface was found to be thermally more stable than the corresponding Pd/GaAs and Pd/Si structures. Comparisons are made between Pd/semiconductor interfacial phenomena on the three semiconductors.

37581 ■ Sorption Mechanisms of Lanthanum on Oxide Minerals

S. Fendorf and M. Fendorf

Clays and Clay Minerals *(in press)*

The retention of hazardous species, including many of the lanthanides, on soils and sediments is vital for maintaining environmental quality. In this study, high-resolution transmission electron microscopy (HRTEM) was used to identify surface precipitates of La and their degree of atomic ordering on oxides of Mn (birnessite), Fe (goethite), and Ti (rutile) over a pH range of 3 to 8. At pH >5.5, the aqueous concentration of La was fully depleted by all three metal oxides. On birnessite, surface precipitation of La-hydroxide occurred at pH $\geq$5 and appears to be the dominant sorption mechanism on this mineral. Surface precipitation was not observed on rutile or goethite until much higher pH values, 6.5 for rutile and 8.0 for goethite. Precipitation is thus correlated with the points of zero charge (PZC) of the minerals (6.3 and 7.8 respectively), and in each case was observed only at pH values above the PZC. Although La sorption was extensive on all the minerals at the higher pHs, the depletion of La from solution by rutile and goethite at pH values well below the PZC indicates that the sorption mechanism differs from that on birnessite, surface complexation of monomeric or small multi-nuclear species appears to predominate for La retention on rutile and goethite at most commonly encountered pH values.

no # **Electron Microscopy of Thin Films Prepared by Laser Ablation**

H. Lemke, C. Echer and G. Thomas

IEEE Trans. Magn. *(submitted)*

A simple processing model has been developed for studying Nd-Fe-B magnets. The grain structure of these samples is comparable to that of melt-spun magnets. The samples are prepared by depositing films on a carbon foil TEM grid by laser ablation. The influence of temperature on the grain structure is emphasized. Deposition at room temperature yields amorphous films. Crystallinity is obtained at heater temperatures above 600°C during deposition. The size of the grains is about 20nm.

38255 ■ **Structure and Morphology of Nanosized Lead Inclusions in Aluminum Grain Boundaries**

E. Johnson, S. Hinderberger, S.-Q. Xiao, U. Dahmen and A. Johansen

Interface Science *(in press)*

Grain boundary lead inclusions formed by ion implantation of mazed bicrystal aluminum films have been investigated by transmission electron microscopy. The vapor-grown bicrystal films contained mainly 90° <110> tilt boundaries with fixed misorientation but variable inclination, as well as some growth twins with 70.5° <110> symmetrical tilt boundaries and a few small-angle boundaries. It was found that the shape, size and orientation of the inclusions in the grain boundaries depend on the orientation of the aluminum grain boundary plane. Inclusions at 90° <110> tilt boundaries were invariably sharply faceted toward one aluminum grain and *more* rounded toward the other grain. The faceted side was a section of the cuboctahedral equilibrium shape of bulk lead inclusions in parallel topotaxy with the aluminum matrix. The rounded side, where the aluminum grain was rotated by 90° with respect to the lead lattice, approximated a spherical cap. At specific low-energy segments of the grain boundary where a (100) plane in grain 1 meets an (011) plane in grain 2, only two of several possible shapes were observed. One of these was preferred in as-implanted samples while both types were found after melting and re-solidification of the lead inclusions. The observations are discussed in terms of a modified Wulff construction.

no # **Silicon Carbide Platelet/Silicon Carbide Composites**

T. Mitchell, Jr., L.C. De Jonghe, W.J. Moberly-Chan and R.O. Ritchie

J. Am. Ceram. Soc. 78 97 *1995*

Alpha-silicon carbide platelet/beta-silicon carbide composites have been produced in which the individual platelets were coated with an aluminum oxide layer. Hot pressed composites showed a fracture toughness as high as 7.2 Mpa.$m^{1/2}$. The experiments indicated that the significant increase in fracture toughness is mainly the result of crack deflection and accompanying platelet pull out. The coating on the platelets also served to prevent the platelets from acting as nucleation sites for the alpha to beta phase transformation, so that advantageous microstructure remains preserved during high temperature processing.

38300 **Zirconium Nitride Precipitation in Nominally Pure Yttria-Stabilized Zirconia**

D. Gómez-García, J. Martínez-Fernández, A. Domínguez-Rodríguez and K.H. Westmacott

J. Am. Ceram. Soc. *(in press)*

Nominally pure yttria-stabilized zirconia alloys are shown to contain unsuspectedly large amounts of dissolved nitrogen. Its presence in the lattice was detected through the observation of large precipitates in alloys with three different concentrations of yttria deformed in compression in argon in the temperature range 1600-1800°C. Electron diffraction, EDS and PEELS analyses and Moiré imaging were used to identify the precipitates as ZrN. The possible origin of the nitrogen, its likely effects on properties and the role of annealing atmosphere are briefly discussed.

38301 ■ **On the Nature of Electron-Beam Induced Loop Formation on Dislocations in Yttria Fully-Stabilized Zirconia**

D. Gómez-García, J. Martínez-Fernández, A. Domínguez-Rodríguez and K. H. Westmacott

J. Am. Ceram. Soc. *(submitted)*

The nature of the strain lobes and loops that form on edge-dislocations in yttria stabilized zirconia during exposure in an electron microscope has been investigated. By changing the operating conditions, such as acceleration voltage, cycling the beam intensity, heating or cooling the specimen prior to observation, or heat treatment prior to the deformation, it has been shown that the effects result from beam heating. During specimen heating ZrN precipitates which have a large misfit with the ZrO_2-Y_2O_3 matrix form in the compressed regions of the dislocation core.

38302 ■ **Microstructure and Ionic Conductivity of Freeze-dried Yttria-doped Zirconia**

M. Filal, C. Petot, K.H. Westmacott, J.Y. Laval, C. Lacour and R. Ollitrault

J. Am. Ceram. Soc. *(submitted)*

The relationship between the microstructure and ionic conductivity of 9mol% yttria-doped zirconia is deduced from a comparative study performed on polycrystalline samples prepared either from commercial powder (sample Z_C) or from freeze-dried powder (sample Z_F). The grain boundary ionic conductivity of the Z_F samples increases with the sintering temperature and this effect is due both to an increase in grain size and to a decrease in the number of glassy triple points. On the other hand, it was found that the grain boundary conductivity of the Z_F sample is 30 times higher than that of the Z_C sample sintered in the same conditions and with the same grain size. According to the microstructural characterizations, this effect seems to be due to the poor microstructure of the Z_C sample and in particular to the presence of a glassy film in a high numnber of grain boundaries. On the contrary, the microstructure of the Z_F samples is cleaner and more homogeneous with larger lens-shaped glassy pockets at triple points.

37569 ■ Polymeric Sol-Gel Synthesis of $La_{1-x}Sr_xMnO_3$ Thin Films Exhibiting Giant Magnetoresistance

A. Modak and K.M. Krishnan

J. Amer. Cer. Soc. *(submitted)*

We report here, for the first time, a reproducible polymeric sol-gel process for the synthesis of $La_{1-x}Sr_xMnO_3$ thin films exhibiting giant magnetoresistance. We have utilized a combination of metal alkoxide, β-diketonate and carboxylate compounds to form the complex precursor which underwent further processing steps of hydrolysis, spin coating and heat treatment. Key features of the process are its overall simplicity, low processing temperature, ease of composition variation, and ability to produce a wide range of structures. The underlying precursor chemistry, leading to atomic scale mixing of elements that occupy the same crystallographic site, critical to the successful synthesis of these films, has also been established. Single phase LSMO(80/20) thin films with a cubic structure (a = 0.38nm) were obtained and confirmed by x-ray diffraction and transmission electron microscopy observations. Epitaxy with (100) normal orientation was induced by deposition on $LaAlO_3$(100) substrates, while polycrystalline thin films were obtained on Si(100) substrates. Magnetoresistance properties comparable to or better than those of films of similar composition obtained by other techniques were observed, further corroborating the feasibility of the process.

37401 ■ Sequential Phase Formation by Ion-Induced Epitaxy in Fe-Implanted Si (001)

X.W. Lin, R. Maltez, M. Behar, Z. Liliental-Weber and J. Washburn

J. Appl. Phys. 78 4382 *1995*

Ion beam induced epitaxial crystallization (IBIEC) of Fe-implanted Si(001) was studied by transmission electron microscopy and Rutherford backscattering spectrometry. For sufficiently high Fe doses, it was found that IBIEC at 320° C results in sequential epitaxy of Fe silicide phases in Si, with a sequence of γ-$FeSi_2$, α-Si_2, and β-Si_2 with increasing Fe concentration along the implantation profile. The critical concentrations for the γ-α and α-β phase transitions were determined as ~11 and 21 at. % Fe respectively. The observed sequential phase formation can be correlated to the degree of lattice mismatch with the Si matrix and the stoichiometry of the silicide phases.

no # ■ **Reaction Mechanism of Cobalt with Silicon Dioxide**

T. Nguyen, H.L. Ho, D.E. Kotecki and T.D. Nguyen

J. Appl. Phys. 79 1123 *1996*

The reaction mechanism of thin cobalt (Co) films with silicon dioxide (SiO_2) substrate under rapid thermal annealing conditions has been investigated. Reaction of thin cobalt film (12.5 nm) with a SiO_2 substrate is observed in an inert ambient (N_2) and in vacuum (~10^{-8} Torr). The reaction is manifested by the formation of craterlike depressions on the SiO_2 substrate and by the presence of a Co_2SiO_4 reaction product determined by transmission electron microscopy diffraction patterns. Much less damage is observed with no reaction product observed if the samples are annealed in a forming gas ambient (90% N_2/10% H_2), the cobalt film is much thicker (150 nm), or the cobalt film is *in situ* cleaned (e.g., 5 min in 400°C, forming gas ambient) prior to annealing in either inert or vacuum ambient. It is proposed that the presence of oxygen is required in order to initiate the reaction between cobalt and SiO_2. The source of the oxygen contaminant, in our studies, is the oxygen on the surface of the cobalt film. The proposed reaction is $2\ Co+SiO_2+2\langle 0\rangle \rightarrow Co_2SiO_4$ where ‹0› represents oxygen contaminant at the surface.

37367 ■ **Epitaxial $Fe_{16}N_2$ Films Grown on Si(100) by Reactive Sputtering**

M.A. Brewer, K.M. Krishnan and C. Ortiz

J. Appl. Phys. *(in press)*

We present a crystallographic template for the growth of the range of Fe-N phases on Si(001) by lattice matching on selected underlayers. Epitaxial films of pure a-Fe, g-Fe_4N and a'-Fe_8N (N martensite) were grown individually by the optimization of reactive N_2 sputtering parameters. The orientation relation of the Fe-N phases was Fe-N(001) || Ag(001) || Si(001) and Fe-N[100] || Ag[110] || Si[100]. Annealing the a'Fe_8N films resulted in the formation of a'-Fe_8N/a"-$Fe_{16}N_2$ mixtures. In addition to the crystallographic and structural analysis, quantification of x-ray diffraction peak intensities confirmed that the a'/a" mixtures contained as much as 46 vol% a" (remaining a'). VSM and SQUID magnetometry measurements of the a' and a'(54%)/a"(46%) mixture, respectively, indicate enhanced magnetic moments for both the a' and a" phases with respect to pure Fe.

37368 ■ Role of Epitaxy and Polycrystallinity in the Magnetoresistance and Magnetization of $La_{0.8}Sr_{0.2}MnO_3$ Thin Films

K.M. Krishnan, A.R. Modak, C.A. Lucas, H.B. Cherry and R. Michel

J. Appl. Phys. *(in press)*

Alkaline earth substituted manganese oxides, $La_{1-x}A_xMnO_3$ (A = Ca, Sr, or Ba), with perovskite structures, have attracted much recent attention because of their very large magnetoresistance for composition in the range $0.1 < x < 0.4$. However, the fundamental mechanism governing their galvanomagnetic properties and magnetization behavior, is, as yet, not understood. Moreover, these properties are observed to be dependent on conditions of growth and annealing, composition, oxidation state, epitaxy and the overall microstructure. More detailed characterization of the structure and properties of these films and the epitaxial growth of similar films with well defined grain boundaries is in progress.

37366 ■ Microstructure and Composition in Rapidly Quenched NdFeB-Based Hard Magnet Alloys

T.D. Nguyen, K.M. Krishnan, L.H. Lewis, Y. Zhu and D.O. Welch

J. Appl. Phys. *(in press)*

A detailed comprehension of the microstructure and composition in NdFeB hard magnet alloys is important in understanding their magnetic properties and reversal mechanisms. In this study, transmission electron microscopy (TEM) studies of the grain boundary phases in melt-quenched, thermomechanically-processed magnet alloys based on the $Nd_2Fe_{14}B$ composition, utilizing high resolution, analytical, and Lorentz techniques, are presented. The relationship between the observed microstructure and magnetic properties, and in particular the reversal mechanism in these materials are discussed.

no # ■ **Change of Structure and Location of Misfit Dislocations in $In_xGa_{1-x}As/GaAs$ (001) System**

Y. Chen, H. Sohn, Z. Liliental-Weber, J. Washburn, J.F. Klem and J.Y. Tsao

J. Appl. Phys. *(submitted)*

The structure and locations of misfit dislocations have been investigated experimentally and theoretically in different strained $In_xGa_{1-x}As$ ($0.2 \leq x \leq 1$) epilayers grown on GaAs substrates. The misfit dislocations in the $In_{0.2}Ga_{0.8}As$ epilayers were predominantly dissociated 60° dislocations with the 90° partials lying in the interface and the 30° partials pushed into the substrate. In $In_{0.3}Ga_{0.7}As$ epilayers, misfit dislocations of both 60° and 90° types were present either in undissociated form or split into partials. These dislocations were not all near the interface; some were scattered through the epilayer. The presence of dislocations of 60° type located away from the interface for intermediate misfits is rationalized by considering the balance of forces acting on these dislocations. In $In_{0.4}Ga_{0.6}As$ and in InAs epilayers, misfit strain was accommodated almost entirely by 90° undissociated dislocations. A model is proposed for the formation of 90° edge dislocations to explain the transition of dominant misfit dislocation type from 60° to 90° type with increasing mismatch.

37722 ■ **Plasma Distribution of Cathodic Arc Deposition Systems**

S. Anders, S.Raoux, K. Krishnan, R.A. MacGill and I. G. Brown

J. Appl. Phys. *(submitted)*

The plasma distribution using a cathodic arc plasma source with and without magnetic macroparticle filter has been determined by depositing on a transparent plastic substrate and measuring the film absorption. It was found that the width of the distribution depends on the arc current, and it also depends on the cathode material which leads to a spatial separation of the elements when an alloy cathode is used. By applying a magnetic multicusp field near the exit of the magnetic filter, it was possible to modify the plasma distribution and obtain a flat plasma profile with a constant and homogeneous elemental distribution which was demonstrated by depositing FeNd thin films.

36167 ■ **Structure and Chemical Composition of a Supported Pt-Ru Electrocatalyst for Methanol Oxidation**

V. Radmilovic, H. Gasteiger and P.N. Ross

J. Catalysis 154 98 *1995*

High resolution electron microscopy (HREM) and x-ray microchemical analysis (EDS) were used to characterize composition, size, distribution and morphology of Pt-Ru particles with nominal Pt:Ru ratio 1:3 and 3:1, supported on carbon black. The particles are predominantly single nanocrystals with diameters in the order of 2.0 to 2.5 nm. Occasionally, twinned particles are also observed. All investigated particles represent solid solutions of Pt and Ru with compositions very close to the nominal one. Based on two-dimensional projection in high resolution images, it is suggested that the well resolved particles are of cubo-octahedral shape. In addition to {200} and {111} facets, {113} facets are also observed.

35968 ■ **Effects of Sodium on the Structure and Fischer-Tropsch Synthesis Activity of Ru/TiO_2**

T. Komaya, Z. Weng-Sieh, R. Gronsky, F. Engelke, T.S. King and M. Pruski

J. Catalysis 152 350 *1995*

The influence of Na on the migration of Ti-containing moieties onto the surface of Ru particles supported on titania has been investigated, together with the effects of Na on the activity and selectivity of titania-supported Ru for Fischer-Tropsch synthesis. It is demonstrated that Na facilitates the decoration and partial encapsulation of Ru by Ti-containing moieties as a consequence of the formation of sodium titanates. Since the Tammann temperature of the titanates is lower than that of the anatase or rutile phases of titania, the temperature at which Ti-containing moieties begin to migrate is reduced in the presence of Na. The turnover frequency for CO consumption based on exposed Ru sites is observed to be independent of the Na content of the catalyst, but the turnover frequency for methane formation decreases monotonically with increasing Na content. The probability for chain growth and the olefin-to-paraffin ration increase and the extent of ethylene reincorporation into the reaction products decrease with increasing Na content. These effects are attributed to a reduction in the surface concentration and mobility of H atoms adsorbed on Ru.

36167 ■ **Structure and Chemical Composition of a Supported Pt-Ru Electrocatalyst for Methanol Oxidation**

V. Radmilovic, H. Gasteiger and P.N. Ross

J. Catalysis 154 98 *1995*

High resolution electron microscopy (HREM) and x-ray microchemical analysis (EDS) were used to characterize composition, size, distribution and morphology of Pt-Ru particles with nominal Pt:Ru ratio 1:3 and 3:1, supported on carbon black. The particles are predominantly single nanocrystals with diameters in the order of 2.0 to 2.5 nm. Occasionally, twinned particles are also observed. All investigated particles represent solid solutions of Pt and Ru with compositions very close to the nominal one. Based on two-dimensional projection in high resolution images, it is suggested that the well resolved particles are of cubo-octahedral shape. In addition to {200} and {111} facets, {113} facets are also observed.

35934 ■ **Carbon Nanostructure in Silica Aerogel Composites**

X.Y. Song, W.-Q. Cao, M.R. Ayers and A.J. Hunt

J. Mat. Res. 10 251 *1995*

In this letter we shall report a new method of preparing carbon nanotubes and their derivatives using silica aerogels as a matrix for the deposition of carbon. We shall present the observation of hollow graphite tubes and rings including nested structures in nanometer dimensions using high resolution transmission electron microscopy. Furthermore, we propose a model for the growth of carbon nanotubes in three steps including nucleation, growth and closure of tubes.

no # ■ **Effect of TiO_2 Doping on Rapid Densification of Alumina by Plasma Activated Sintering**

R.S. Mishra, A.K. Mukherjee, K. Yamazaki and K. Shoda

J. Mat. Res. *(in press)*

The effects of plasma cycle and TiO_2 doping on sintering kinetics during plasma activated sintering (PAS) of g-Al_2O_3 have been studied in the temperature range of 1473-1823 K. Multiple plasma cycle leads to higher densification. Also, TiO_2 doping enhances the sintering kinetics during PAS. In TiO_2 doped specimens, near full density was obtained at 1673 K in less than 6 minutes using multiple plasma cycle. It is suggested that the dielectric properties of a material are critical for the success of the PAS process.

36193 ■ **Phase Transformation and Microstructural Changes of Si_3N_4 During Sintering**

Y. Goto and G. Thomas

J. Mat. Sci. 30 2194 *1995*

Changes of density, the α-β phase transformation, and composition of grains and grain-boundaries during sintering of Si_3N_4 with various sintering conditions using additives of Y_2O_3 and Al_2O_3 were investigated. The phase determination of individual Si_3N_4 grains was performed by convergent beam electron diffraction (CBED). The relations between densification and transformation were divided into two groups, depending on the additive compositions. Al dissolution into Si_3N_4 grains occurred mostly during the α-β transformation process. The concentration of Al and O in the grain boundaries decreased as the α to β transformation progressed.

35858 **In-Situ High-Resolution Electron Microscopy Observations of Nanometer-Sized Pb Inclusions in Al Near Their Melting Point**

S.Q. Xiao, S. Hinderberger, U. Dahmen, E. Johnson, A. Johansen and K.K. Bourdelle

J. Microscopy 180 Pt. 1 61-69 *1995*

Nanometer size Pb precipitates were produced by implantation of Pb ions at 40 keV into Al thin films at 150° C. Both Pb and Al are face centered cubic and the precipitates invariably adopted the cube-cube orientation relationship. The shape of most precipitates was close to a cubo-octahedron, faceted on eight [111] and six [100] interfaces. *In-situ* HREM observations of the precipitates were made near a <110> common zone axis and the thermal behavior was recorded on video tape. The precipitates inside the grains remained solid up to ~30° C above the bulk melting point of lead (327° C). The melted precipitates remained as liquid inclusions due to the lack of solubility of lead in Al. Resolidification of the precipitates began to take place when the sample was cooled to around the bulk melting point of lead. Morphologies of the lead precipitates as well as atomic-scale changes associated with the melting and resolidification were recorded and analyzed on video and HREM micrographs.

no # **Quantification of the modulated structures in TiPdCr alloys**

A.J. Schwartz, S. Paciornik, R. Kilaas and L.E. Tanner

J. Microscopy 180, Pt. 1 51-60 *1995*

Using a newly developed method for quantifying atomic displacements from HRTEM images, the natures of modulated phases in Ti50Pd(50-x)Crxß2 alloys have been investigated as part of an overall study of the systematics of phase transformation behavior. In modulated phases of Ti50Pd43Cr7 and Ti50Pd42Cr8 alloys, the atoms are shifted from the cubic lattice by a transverse lattice displacement wave. The atomic displacements were determined and compared to truly incommensurate and varying three- and four-plane wave packets using correlation coefficients for a least squares fit. The results indicate that the modulations are probaly incommensurate in nature.

37890 ■ **Symmetry of Annealed Wurtzite CdSe Nanocrystals: Assignment to the C_{3v} Point Group**

J.J. Shiang, A.V. Kadavanich, R.K. Grubbs and A.P. Alivisatos

J. Phys. Chem. 99 17419 *1995*

High-resolution electron microscopy and resonance Raman spectroscopy are used to assign annealed wurtzite CdSe nanocrystals to the C_{3v} point group. Deviations from spherical symmetry have spectroscopic consequences for this prototypical quantum dot system.

37156 ■ **Ge/Si Heterostructures Grown by Sn-Surfactant-Mediated Molecular Beam Epitaxy**

X.W. Lin, Z. Liliental-Weber, J. Washburn, E.R. Weber, A. Sasaki, A. Wakahara and T. Hasegawa

J. Vac. Sci. Techn. B 13 1805 *1995*

Ge/Si heterostructures were grown on Si (001) by Sn-submonolayer-mediated molecular beam epitaxy (MBE) and characterized by a variety of techniques, in order to study the behavior of Sn surfactant during Ge and Si growth and its influence on Ge/Si interface quality. It was found that Sn strongly segregates to the growing surface of both Ge and Si and that the presence of Sn surfactant can effectively suppress Ge segregation into a Si overlayer and enhance the surface mobility of adatoms. These results suggest that Sn-mediated epitaxy can be used as a viable method to produce Ge/Si superlattices, with an interface quality superior to those grown either by conventional MBE or with other types of surfactants.

37035 ■ Electron Microscopy Characterization of GaN Grown by MBE on Sapphire and SiC

Z. Liliental-Weber, H. Sohn, N. Newman and J. Washburn

J. Vac. Sci. Technol. 13 1578 *1995*

Transmission electron microscopy was used for the characterization of GaN epitaxial layers grown by molecular beam epitaxy on two different substrates: sapphire (Al_2O_3) and 6H-SiC. GaN layers grown on both substrates crystallize with the wurtzite structure. Despite the very different lattice mismatch associated with their two substrates, similar types of defects were formed in the GaN layer, only their density differed. In addition to small angle sub-grain boundaries, two other types of defects were seen in cross-sectioned samples: defects parallel to the growth surface and microtwins with a width of about 8-10 nm perpendicular to the growth surface. The parallel defects were identified as stacking faults leading to local fcc atom arrangement in the layer and are believed to be growth defects. The density of these faults decreased with layer thickness. However, the density of the vertical microtwins remained constant through the layer. Slight local lattice twist between the microtwin and surrounding areas or differences of stoichiometry are suggested as an explanation for the observed contrast of the high resolution images.

37597 ■ Metallurgy of Al-Ni-Ge Ohmic Contact Formation on n-GaAs

X.W. Lin, W.V. Lampert, T.W. Haas, P.H. Holloway, Z. Liliental-Weber, W. Swider and J. Washburn

J. Vac. Sci. Technol. B 13 2081 *1995*

Al-Ni-Ge ohmic contacts on n-GaAs were prepared by sequential vapor deposition and furnace annealing at 500° C. The metallurgical properties of the contacts were studied by transmission electron microscopy. It was found that while Al-Ni-Ge as a whole is relatively stable against GaAs, extensive interfacial reactions readily occur within the contact layers, resulting in a very stable layered structure of the type Al_3Ni/Ni-Ge/GaAs, with ε'-Ni_5Ge_3 being the major phase in the Ni-Ge layer. GaAs twins and Ni-As precipitates were found in a thin layer immediately below the metallization, suggesting that the ohmic behavior can be accounted for in terms of a GaAs regrowth mechanism.

no # ■ **Phase Behavior of Ordered Diblock Copolymer Blends: Effect of Compositional Heterogeneity**

R.J. Spontak, J.C. Fung, M.B. Braunfeld, J.W. Sedat, D.A. Agard, L.Kane, S.D. Smith, M.M. Satkowski, A.Ashraf, D.A. Hajduk and S.M. Gruner

Macromolecules *(submitted)*

Diblock copolymers order into a variety of periodic morphologies when $c N > (c N)_{ODT}$, where c is the Flory-Huggins interaction parameter, N is the number of statistical segments, and ODT denotes the order-disorder transition. Previous studies have demonstrated that classical dispersion (spherical and cylindrical) and lamellar morphologies, as well as novel complex morphologies (*e.g.*, gyroid*, lamellar catenoid, and hexagonally perforated lamellae), can be selectively accessed through either tailored molecular synthesis or copolymer/homopolymer blends. In the present work, control over ultimate morphology is achieved through the use of binary copolymer blends composed of two strongly-segregated poly (styrene-*b* -isoprene) (SI) diblock copolymers of comparable N but different compositions. Blend morphologies are examined by electron microscopy (including 3-dimensional imaging) and small-angle x-ray scattering, and a theoretical framework is proposed to describe strongly-segregated blends exhibiting the lamellar morphology. Results obtained indicate that diblock copolymer blends behave as neat diblock copolymers of equal bulk composition, suggesting that such blends offer an alternative, and attractive, route by which to generate a desired morphology.

none ■ **Architecture-Induced Phase Immiscibility in a Diblock/ Multiblock Copolymer Blend**

R.J. Spontak, J.C. Fung, M.B. Braunfeld, J.W. Sedat, D.A. Agard, A. Ashraf and S.D. Smith

Macromolecules *(submitted)*

Ordered diblock copolymer blends have recently become a subject a tremendous research interest since they can be used to elucidate intramicrodomain segregation of blocks differing in length, as well as to identify the molecular and blend parameters yielding phase immiscibility. In this work, we explore the influence of molecular architecture on block copolymer blend miscibility by examining an equimolar mixture of two symmetric styrene (S)/isoprene (I) block copolymers, one an SI diblock and the other an $(SI)_4$ octablock. Their molecular weights are identical so that the ratio of block lengths is 4:1 SI:$(SI)_4$. While this ratio is expected to yield a single phase in diblock copolymer blends, transmission electron microscopy reveals here that the diblock/multiblock blend is macrophase-separated due to the linear multiblock architecture and midblock conformations of the $(SI)_4$ microdomains at the SI/$(SI)_4$ interface at relatively high spatial resolution (*ca.* 3 nm). In addition, the presence of SI molecules in the $(SI)_4$ phase or $(SI)_4$ molecules in the SI phase frustrates SI lamellae, resulting in curved microphase boundaries.

no # ■ **In-Situ Deformation of Aluminium Alloy Polycrystals Observed by High-Voltage Electron Microscopy**

J.M. Robinson

Mat. Sci. and Eng. (A) 203 238 *1995*

In-situ deformation of aluminium alloy polycrystals has been investigated within a high-voltage transmission electron microscope in order to observe dislocation phenomena related to the Portevin-Le Chatelier effect. The alloys examined are commercially pure aluminium, binary Al-2 at.% Ag, Al-2 at.% Zn, Al-2 at.% Mg and a commercial alloy containing approximately 5 at.% Mg. All the materials tested exhibit flow-stress discontinuities during room temperature deformation, although the amplitude of serrations is substantially higher in the material containing Mg. In-situ deformation is correspondingly discontinuous in all cases but the coordination of dislocation motion in the material containing Mg is markedly high. Deformation in all the material examined is characterised by the sudden activation and collective motion of multiple dislocations, but this is predominantly confined to a single-slip system in the case of alloys containing Mg. In contrast, alloys which do not contain Mg exhibit concurrent, dispersed slip on multiple intersecting slip systems characterised by extensive cross-slip.

no # ■ **In Situ Ultra-High Vacuum Transmission Electron Microscopy Studies of Nanocrystalline Copper**

D.L. Olynick, J.M. Gibson and R.S. Averback

Mat. Sci. and Eng. (A) 204 54 *1995*

We have built a particle production and transport system that allows the characterization of nanocrystals without exposure to contaminating atmospheres such as air. Nanocrystals (formed by inert gas condensation of a sputtered atom population) are transported in situ via the gas phase to an ultra-high vacuum transmission electron microscope (UHVTEM) equipped with a heating stage and gas exposure system. With this system, we can study various nanoparticle phenomena in real time and under clean conditions. In this paper we discuss the experimental design and preliminary studies using imaging and diffraction techniques. These include, the time-evolution of copper nanoparticle morphology and sintering behavior as a function of particle size, temperature, oxygen/atmosphere exposure and supporting substrate. In particular, we have observed immediate room temperature sintering of dean copper nanocrystals which does not occur with nanoparticles that have been exposed to oxygen. Furthermore, we have seen an interaction between copper nanocrystals and amorphous carbon which produces graphite shells. This shell formation process suggests a solid state analog to that seen when nanoparticles catalyze the growth of carbon fibers through a hydrocarbon atmosphere decomposition.

35891 ■ **Studies on Ordered Mesoporous Materials III: Comparison of MCM-41 to Mesoporous Materials Derived from Kanemite**

C.-Y. Chen, S.-Q. Xiao and M.E. Davis

Micropor. Mats. 4 1 *1995*

MCM-41 and mesoporous materials derived from kanemite are synthesized and characterized by x-ray powder diffraction (XRD), N_2 adsorption/desorption, cyclohexane and water physical adsorption, scanning electron microscopy (SEM), transmission electron microscopy (TEM), thermogravimetric analyses (TGA, FTIR and ^{13}C and ^{29}Si MAS NMR spectroscopy. Both preparations yield mesoporous materials with narrow pore size distributions and somewhat similar physicochemical properties. However, due to a higher degree of condensation in the silicate walls of the materials derived from kanemite, these samples have higher thermal and hydrothermal stability than MCM-41. Additionally, the mechanisms by which these two types of materials are formed are dramatically different.

35859 ■ **Preparation of Oxide Superconductor Specimens for TEM Examination**

M. Fendorf, M. Powers and R. Gronsky

Micros. Res. & Techn. 30 167 *1995*

We have investigated a wide variety of oxide superconductors, and report here on a number of techniques that can be effectively used to prepare TEM specimens from these materials. Crushing, cleaving, ion milling, ultramicrotomy, and jet polishing all were successfully utilized, and details of each technique, as well as equipment used, are described. Selection among these methods depends both on the starting form of the material and on the information required. Ion milling and crushing generally give the best results and have the widest applicability in our particular work, while crushing and cleaving involve the least equipment cost. In some cases, particularly with ion milling and jet polishing, small variations in the details of preparation have a dramatic effect on the success rate. We have found it to be a great advantage that the same techniques can be applied in a similar manner to a whole range of oxide materials, even (with some refinements and special precautions) to those which are extremely oxygen or moisture sensitive.

37175 ■ A Method for Jet Polishing Two-Phase Materials

M.J. Witcomb and U. Dahmen

Micros. Res. & Techn. 32 70 *1995*

A two-phase jet polishing technique is described, which, utilizing the effects of the characteristic current-voltage behavior of electropolishing solutions, can produce excellent TEM foils of relatively coarse two-phase materials.

37583 ■ Magnetism on a Microscopic Scale

K.M. Krishnan

MRS Bulletin 20 24 *1995*

Tremendous progress has been made in the field of magnetic materials research and technology over the past few years. Superior properties and novel scientific questions arise due to our ability to either synthesize artificial structures or to tailor microstructures at the appropriate length scale. The development of enhanced macroscopic properties in such materials requires, in addition to synthesis, that the magnetic microstructure be quantitatively determined and its dependence on the physical/chemical microstructure, at the appropriate length scale, understood. Such studies are also motivated by the technologies of information storage, magnetic and magneto-optic recording, sensors and magnetic devices. Whilst these applications have been the focus of earlier issues of the MRS bulletin, here we emphasize the physics, materials sciences, novel magnetic measurements, micromagnetics and the implications of the above on emerging technologies. In summary, these articles are a representative "snap shot" of the exciting area of research in magnetism on a microscopic scale, and the contributors have managed to convey details of both the fundamental phenomena being addressed and the unique techniques they have developed (and continue to develop) to study them at the appropriate length scales.

no # ■ **SPLEEM of Magnetic Surfaces and Layered Structures**

H. Poppa, E. Bauer and H. Pinkvos

MRS Bulletin 20 38 *1995*

SPLEEM is a new imaging approach for the analysis of magnetic microstructures on solid surfaces under UHV conditions. The lateral-image resolution is of the order of 10 nm and is therefore comparable to that of the SEMPA technique as well as being superior to light optical Kerr and scanning magnetic force microscopy (MFM). The most intriguing feature of SPLEEM is its imaging speed, which permits high-resolution monitoring of kinetic changes of magnetic-surface structures. In previous versions of SPLEEM, only in-plane magnetizations could be detected; in the latest instrument version, all magnetization directions can be studied. When SPLEEM is combined with in situ vapor deposition and surface analytical facilities, it becomes possible to investigate the nucleation and growth of magnetic monolayers and multilayers with unequaled versatility and precision.

37752 ■ **Applications of Electron Microscopy to Industrial Research**

F.M. Ross, K.M. Krishnan, N. Thangaraj, R.F.C. Farrow, R.F. Marks, A. Cebollada, S.S.P. Parkin, et al.

MRS Bulletin *(submitted)*

The transmission electron microscope (TEM) is one of the most successful tools available to the materials scientist. Yet both the complexity and expense of the equipment, and the huge investment in time necessary to become proficient in specimen preparation and image acquisition and analysis, mean that it is difficult for most industrial institutions to maintain a state-of-the-art TEM facility. How can industry overcome this problem? One solution is to set up a collaboration with a university, an industrial partner or a government research laboratory. Such a collaboration can be extremely valuable to the company, which gains access to microscopes, specimen preparation equipment and the expertise of professional microscopists, and to the research laboratory, which benefits from the industrial perspective and the private sector's proficiency in materials preparation and processing. In this paper we present three case studies of successful collaboration between industry and the National Center for Electron Microscopy.

38256 ■ **An Electron Microscopy Study of Nanocrystalline ZrO_2**

W. Dickenscheid, S-Q. Xiao, U. Dahmen and R. Birringer

Nanostructured Materials *(submitted)*

The microstructure of nanocrystalline ZrO_2 generated by inert-gas condensation and post oxidation has been characterized by energy dispersive spectroscopy (EDS), selected area electron diffraction (SAD), and high resolution electron microscopy (HREM). The alloy is composed mainly of a metastable (cubic or tetragonal) ZrO_2 phase with grain sizes ranging from 5nm to 40nm. Dislocations have been observed in grains down to 9nm and their number as a function of the grain size was measured. From these data the average dislocation density for the different grain size regimes was calculated to be between $1*10^{15}$ and $5.5*10^{15}$ per m^2 .

no # ■ **Fully Collapsed Carbon Nanotubes**

N.G. Chopra, L.X. Benedict, V.H. Crespi, M.L. Cohen, S.G. Louie and A. Zettl

Nature 377 135 *1995*

It has been suggested that the tensile strength of carbon nanotubes might exceed that of other known fibers because of the inherent strength of the carbon-carbon bond. Calculations of the elastic properties of nanotubes confirm that they are extremely rigid in the axial direction and are most likely to distort perpendicular to the axis. Carbon nanotubesa with localized kinks and bends, as well as minor radial deformations, have been observed. Here we report the existence of multi-shelled carbon nanotubes whose overall geometry differs radically from that of a straight, hollow cylinder. Our observations reveal nanotubes that have suffered complete collapse along their length. Theoretical modeling demonstrates that, for a given range of tube parameters, a completely collapsed nanotube in favored energetically over the more familiar "inflated" form with a circular cross-section.

36902 ■ Morphology and Interface Structure of Mo_5Si_3 Precipitates in $MoSi_2$

S.Q. Xiao, S.A. Maloy, A.H. Heuer and U. Dahmen

Phil. Mag. A 72 997 *1995*

Two distinctly different morphologies of Mo_5Si_3 precipitates have been observed in a single crystal $MoSi_2$. Both precipitates are laths elongated along the <110> direction common to the matrix and the precipitate, but differ in their cross-sectional shape and lattice orientation. Type I precipitates exhibit a rectangular cross section, with interfaces parallel to low-index planes $(110)_m \parallel (002)_p$ and $(002)_m \parallel (220)_p$, while type II precipitates are parallelograms, with their major interface at 13° to the low-index planes $(002)_m \parallel (220)_p$, (the subscripts m and p denote the $MoSi_2$ matrix and Mo_5Si_3 precipitate, respectively). The orientation relationships corresponding to the two characteristic morphologies differ by a 1.8° rotation around the lath axis. A periodic array of dislocation loops and associated ledges enveloping the precipitates were revealed by high resolution electron microscopy and selected area electron diffraction. The Burgers vector of these dislocations was determined umambiguously from high resolution images in orthogonal viewing directions. The differences between the two characteristic morphologies and their orientation relationships are due to a difference in the stacking sequence of ledges.

37595 ■ The Effect of Twinning on the Shapes of Cube-Cube Related Ge Precipitates in Al

S.Q. Xiao, S. Hinderberger, K.H. Westmacott and U. Dahmen

Phil. Mag. A *(in press)* *1996*

This work establishes a correlation between the shape and internal twin structure of cube-cube related Ge precipitates in Al. Using conventional and high resolution electron microscopy, it is shown that most triangular plates have only one twin variant, parallel to the habit plane. Hexagonal plates have two or more twins of the same variant, parallel to the habit plane. Most tetrahedral precipitates have two non-coplanar twin variants. Small octahedral precipitates are twin-free, while larger octahedra can have up to 2 twin variants. The different shapes are due to preferential growth at grooves formed by reentrant twin junctions, and an increased mobility of the interfaces between the matrix and a twinned precipitate. It is shown that precipitates nucleate as twin-free octahedra. The effect of single, double and secondary twinning on precipitate growth is analyzed systematically, and compared with experimental observations. Symmetry considerations show that all three precipitate forms are consistent with Curie's principle if the de-symmetrizing effect of twinning is taken into consideration.

38097 ■ Transmission Electron Microscopy of the AlN/SiC Interface

F.A. Ponce, M.A. O'Keefe and E.C. Nelson

Phil. Mag. A *(in press)*

The AlN/SiC interface has been studied using high resolution transmission electron microscopy. Cross section lattice images of the AlN/SiC interface have been analyzed to establish the connection between image contrast and the atomic positions in the lattice. Assuming atomically abrupt and planar AlN/SiC interfaces, four possible atomic bonding configurations are taken into account for SiC substrates with the (0001)Si orientation. Image simulations of these four interface models are compared with the experimental images. Considering variations at the interface of the image contrast, the basal-plane distance, and the projected charge density, it is shown that the C-Al and Si-N bonds are in agreement with the experimental images and are not distinguishable under our experimental conditions. The other two possibilities, involving C-N and Si-Al bonds, are not consistent with our observations.

37723 ■ Porous Gallium Arsenide and Porous Silicon: A Comparison

F.M. Ross, G. Oskam, P.C. Searson, J.M. Macaulay and J.A. Liddle

Phil. Mag. A *(submitted)*

The structure of porous layers formed in n-type gallium arsenide is characterized and compared with the more familiar structure of porous n-type silicon formed under analogous conditions. Although similar in many respects, the pores formed show characteristic differences which provide insight into the pore formation process. The morphology is discussed in terms of a simple model in which we consider the bonding configuration of atoms on steps, kinks and terraces on the interior of the pore and the spatial distribution of the rate-limiting electrochemical reactions.

38257 **Phase Transformation of TiO_2 Precipitates in Sapphire Induced by the Loss of Coherency**

S.Q. Xiao, U. Dahmen and A.H. Heuer

Phil. Mag. A *(submitted)*

The first phase to precipitate in Ti-doped sapphire (a-Al_2O_3) single crystals annealed at 1300°C in air is a high pressure form of titanium dioxide with the a-PbO2 structure (a-TiO_2). The precipitates form as oblate spheroidal plates with habit planes parallel to $(0001)_s$. Because the a-TiO_2 precipitates are coherent with the sapphire matrix when small, they are under compressive stress resulting from a 5% lattice mismatch with sapphire. During coarsening they lose coherency by emitting a dislocation loop with a 1/3<1101>s Burgers vector. The loss of coherency reduces the stress on the precipitates, and allows them to transform to the rutile structure. The orientation relationship between the sapphire matrix, a-TiO_2 and rutile has been determined and a lattice correspondence for the phase transformation proposed. Although the transformation from a-TiO_2 to rutile is purely structural, its rate is controlled by diffusion because the increased atomic volume of rutile is accommodated by expelling extra mass into the nearby dislocation loop, and is associated with a change in the precipitate shape.

38372 **Morphology, Structure and Thermal Behavior of Small Eutectic Pb-Cd Inclusions in Aluminum**

S. Hagège and U. Dahmen

Phil. Mag. Lett. *(submitted)*

Small inclusion of eutectic Pb-Cd embedded in a solid Al matrix were produced by melt spinning and investigated by transmission electron microscopy. Inclusions were found to be phase separated into two parts, one face-centered cubic and Pb-rich, the other hexagonal close-packed and Cd-rich. The two phases maintained an orientation relationship of parallel close-packed planes and directions with each other and with the fcc Al matrix. The inclusion shape was anisotropic and each segment displayed the facets typical for pure Pb and pure Cd inclusions found in binary Al-Pb and Al-Cd alloys. Within the observed size range of 5 to 100 nm, particles exhibited a single Pb-Cd interface, invariably parallel to the shared close-packed plane. The bimetal inclusions were found to melt at the eutectic bulk melting point regardless of size. Melting was initiated at the triple interface junction of Cd, Pb and Al. By comparison, solidification during cooling required an undercooling of about 35°C and took place very rapidly in less than 1/30 s. The volume change during solidification led to an elastic distortion of the surrounding matrix which subsequently decayed over a period of over 20s.

36862 **The Role of Elasticity Associated with Oxygen Ordering in $YBa_2Cu_3O_z$**

M. Goldman, C.P. Burmester, L.T. Wille and R. Gronsky

Phys. Rev. B 52 1331 *1995*

A Monte Carlo technique incorporating elasticity is applied to simulate oxygen-vacancy ordering and concomitant elastic distortion within the basal plane of $YBa_2Cu_3O_z$. Simulations performed with this model are first compared to previous studies of oxygen-vacancy ordering under a static lattice approximation, and then used to investigate the contribution of elastic strain to the formation of experimentally observed $\sqrt{2}$ superstructures, deformation tweed, twinning, nucleation and growth of ordered domains, and the nature of the tetragonal-to-orthorhombic transition occurring in this system. The influence of elasticity on microstructural evolution is examined via simulations of rapid quenching through the tetragonal-to-orthorhombic transition or of deformation of the orthorhombic phase to induce strain, both followed by annealing. The formation and evolution of these microstructures are rationalized in terms of the accommodation of strain energy accumulated during the course of the simulated thermo-mechanical treatments.

37817 **Sn Submonolayer-Mediated Ge Heteroepitaxy on Si (001)**

X.W. Lin, Z. Liliental-Weber, J. Washburn, E.R. Weber, A. Sasaki, A. Wakahara and T. Hasegawa

Phys. Rev. B. 15 *1995*

The influence of a Sn submonolayer on the growth mode of Ge on Si (001) during molecular beam epitaxy has been studied by transmission electron microscopy and reflection high-energy electron diffraction. It was found that Sn-mediated growth promotes Ge island formation, suggesting that Sn acts to enhance the surface mobility of Ge adatoms. It is pointed out that being able to uniformly cover and strongly segregate to the growing surface is necessary, but not sufficient, for a surfactant to effectively suppress Ge islanding on Si.

38243 **Size, Shape and Composition of Luminescent Species in Oxidized Si Nanocrystals and H-Passivated Porous Si**

S. Schuppler, S.L. Friedman, M.A. Marcus, D.L. Adler, Y.-H. Xie, F.M. Ross, et al.

Phys. Rev. B 52 4910 *1995*

Near edge and extended x-ray absorption fine-structure measurements from a wide variety of oxidized Si nanocrystals and H-passivated porous Si samples, combined with electron microscopy, ir absorption, forward recoil scattering, and luminescence emission data, provide a consistent structural picture of the species responsible for the luminescence observed in these systems. For porous Si samples whose luminescence wavelengths peak in the visible region, i.e., at <700nm, their mass-weighted-average structures are determined here to be particles (not wires), whose short-range character is crystalline and whose dimensions — typically <15 Å — are significantly smaller than previously reported or proposed. Results are also presented which demonstrate that the observed visible luminescence is not related to either a photo-oxidized Si species in porous Si or an interfacial suboxide species in the Si nanocrystals. The structural and compositional findings reported here depend only on sample luminescence behavior, not on how the luminescent particles are produced, and thus have general implications in assigning quantum confinement as the mechanism responsible for the visible luminescence observed in both nanocrystalline and porous silicon.

38098 **Observation of Competing Etches in Chemically-Etched Porous Silicon**

M.J. Winton, S.D. Russell and R. Gronsky

Phys. Rev. Lett. *(submitted)*

Analyses of the surface morphology of chemically-etched, light-emitting porous silicon reveal distinctive evidence that the porous silicon "stain etch" is actually two competing ones: a localized etch that forms the porous nanostructure, and a delocalized etch that removes material on a much coarser scale. It may be possible, using this knowledge, to tailor a surface that is more amenable to deposition of contact layers. The dominant etch appears to be dependent primarily upon the availability of holes, which are required for porous silicon formation.

36238 ■ TEM Investigation of Multilayered Structures in Heterogeneous Au-Co Alloys

J. Bernardi, A. Hütten, S. Friedrichs, C.E. Echer and G. Thomas

Phys. Stat. Sol. A 147 165 *1995*

The microstructure of melt-span $Au_{83.3}Co_{16.7}$ and $Au_{71.6}Co_{28.4}$ ribbons is investigated by means of analytical and high-resolution electron microscopy. The as-quenched ribbons contain a multilayered lamellar eutectic within the grains and Co precipitates at grain boundaries. Cobalt-rich lamellae are found with growing direction <110> and an average width of 7.5nm. The thickness of the Co-lamella parallel to [001] is larger in the sample with the higher Co-content. Annealing at 480° C dissolves the eutectic and large Co particles are formed at grain boundaries and within the grains deteriorating the magnetic properties.

37598 ■ Lorentz Microscopy of Giant Magnetoresistive Au-Co Alloys

A. Hütten, J. Bernardi, C. Nelson and G. Thomas

Phys. Stat. Sol. A 150 171 *1995*

The magnetic domain structure of melt-spun giant magnetoresistant $Au_{71.6}Co_{28.4}$ samples in as-prepared and annealed states is determined by means of Lorentz microscopy using the JEOL-1000 atomic resolution microscope (ARM) in a modified diffraction mode. The interpretation of the domain structure is done by comparing magnetic contrasts observed in Fresnel mode with simulated contrasts using a geometrical algorithm based on the Lorentz equation. Cobalt precipitates 50 to 100 nm in diameter are found in a single domain state with a curling-like magnetization, that reduces their magnetic stray fields. Large precipitates (~200 nm) are multidomain particles.

35853 **Microstructure and Giant Magnetoresistance in Granular and Multilayer Magnetic Thin Films**

N. Thangaraj, K.M. Krishnan and R.F.C. Farrow

Scr. Met. et Mat. 33 1667-77 *1995*

The microstructure and magnetic properties of phase-separated (FeAg, CoAg) granular and multilayer Permalloy (Py)/Au magnetic thin films exhibiting giant magnetoresistance (GMR) have been investigated. Surprisingly, two Fe-Ag films of similar composition grown under identical conditions and having substantially different microstructures yet display similar GMR. The microstructure of these films is characterized by Fe-rich or Co-rich regions respectively, 350-700 nm in extent and surrounded by a Ag-rich matrix. Essentially pure fcc Co particles and bcc Fe particles of ~15 to 25Å in diameter account for the GMR exhibited by these alloys. This suggests that a size distribution of magnetic particles, sharply peaked at the optimum size with limited bulk segregation, might give rise to larger GMR values. HREM analysis of as-grown permalloy (Py)/Au multilayers in (111) orientation revealed that the Au and Py layers have sharp interfaces with defects such as twin boundaries and misfit dislocations. On mild annealing, the twin density decreases and the multilayer interfaces become rough. The magnetoresistance of the as-grown Py/Au multilayer decreased from 11% to 8% on annealing at 250°C for 40 minutes.

no # ■ **Processing of Nanostructured Nickel by Severe Plastic Deformation Consolidation of Ball-Milled Powder**

R.Z. Valiev, R.S. Mishra, J. Groza and A.K. Mukherjee

Scr. Met. et Mat. *(in press)*

Recent investigation shows that severe plastic deformation, i.e., intense plastic deformation with true logarithmic strains about 5 - 7 under high pressure, is capable of both refining and effectively consolidating ordinary powders of metals and ceramics. In this respect, the process of severe plastic deformation consolidation (SPDC) of nanocrystalline powders produced by ball-milling (BM) seems very promising because of two main reasons. First, the present methods of effective consolidation of ball-milled powders (which are very hard) into bulk samples that possess both full density and retain nanocrystalline structure have not been attained up until now. Second, due to additional energy introduced by SPDC, one can expect to get nanostructures with very high (close to the limit) density of lattice defects and, therefore, to obtain rather unusual structure and properties. This paper presents results of synthesis and the first structural studies of nanocrystalline nickel, prepared by consolidation of ball-milled powder by means of severe plastic deformation.

no # ■ **Influence of Temperature on Segregation in 2009 Al-SiC_w Composite and Its Implication on High Strain Rate Superplasticity**

R.S. Mishra, C. Echer, C.C. Bampton, T.R. Bieler and A.K. Mukherjee

Scr. Met. et Mat. *(in press) 1996*

The high strain rate superplasticity in 2009 Al-SiC_w composite is influenced by prior thermomechanical history. The influence of temperature on segregation in 2009 Al-SiC_w composite has been studied for the first time by in-situ transmission electron microscopy to establish the nature of segregation at high temperature. Contrary to some suggestions in the literature, in-situ analysis at room temperature and 500°C revealed that chemical inhomogeneity in the matrix and interfaces observed at room temperature disappear at 500 °C. The precipitates were observed to dissolve and the results agree well with the differential thermal analysis results. These results are also consistent with the theoretical expectation of dissolution of precipitates during heating above the solvus temperature. No elemental segregation was observed in this composite at room temperature. The implication of these results is that the mechanism of high strain rate superplasticity in aluminum alloy matrix composites is more likely to be microstructure related as compared to liquid phase assisted.

no # ■ **Structural Characterization of Bulk GaN Crystals**

Z. Liliental-Weber, C. Kisielowski, X. Liu, L. Schloss, J. Washburn, E.R. Weber, I. Grzegory, M. Bockowski, J. Jun, T. Suski et al.

Sol. State Elec. *(in press)*

TEM characterization of bulk GaN crystals grown at 1500-1800K in the form of plates from a solution of atomic nitrogen in liquid gallium under high nitrogen pressure (up to 20 kbars) is described. The plate thickness along the c axis was about 100 times smaller than along the nonpolar growth directions. A substantial difference in material quality was observed near the two opposite sides of the plates normal to the c direction. This was related to the polarity of the crystal. On one side the surface was almost atomically flat and the underlying material was free of any extended structural defects, while the other side was rough. The planar defects (dislocation loops and stacking faults formed on the basal planes) near the rough side of the crystal did not have a substantial influence on the FWHM of x-ray rocking curves. A large difference in crystal stoichiometry was observed in different sublayers of the crystals. Based on convergent beam electron diffraction and cathodoluminescence it was proposed that GaN antisite defects are related to the yellow luminescence observed in these crystals.

38402 ■ **Cross-Sectional High Resolution Transmission Electron Microscopy of the Microstructure of Electrochromic Nickel Oxide**

X.Y. Song, Y.X. He and C.M. Lampert

Solar En. Mat. /Solar Cells *(submitted)*

Electrochromic nickel oxide films on indium tin oxide (ITO) were investigated by cross section high resolution transmission electron microscopy and energy dispersive x-ray analysis. Microstructural features and the differences between high quality and poor quality samples were studied and compared. The dominant phase of the NiO film has cubic structure, but selected area electron diffraction patterns revealed many extra diffraction spots for the high performance samples which may result from additional hydrated nickel oxide phases. The NiO grains do not show clear shapes in the cross section plane nor are there signs of a preferred orientation. The mean grain size is larger and there are more defects and superlattices in samples with good electrochromic properties. There was a clear correlation between grain size distribution and performance. The high quality samples had a mean grain size of about 6.5nm, whereas the poor quality samples exhibited significantly smaller mean grain sizes of 5.0 and 3.8 nm.

36753 ■ **A Pattern Recognition Technique for the Analysis of Grain Boundary Structure by HREM**

S. Paciornik, R. Kilaas, J. Turner and U. Dahmen

Ultramicroscopy *(in press)*

A pattern recognition technique for the detection of structural units in high resolution images of interfaces is described. The technique uses cross correlation functions as a means of locating atomic patterns characteristic for an interface and as a measure of similarity between related units. Application is not limited to periodic, or even to planar interfaces. Characteristic structural units can be extracted from an experimental image and some important parameters such as mirror or mirror glide symmetry, and rigid body displacements can be determined without knowledge of the imaging parameters. The technique allows an image of a structural unit with reduced specimen noise to be obtained by averaging over several similar units, even if a boundary is not periodic and not planar. Characteristic structural units so determined can subsequently serve as a basis for structure determination by a refinement process image simulation optimized for several experimental parameters.

37770 ■ Effect of Pre-Aging on the Evolution of Ge Precipitates in an Al-1.8 at % Ge Alloy

S. Hinderberger, S.-Q. Xiao, K.H. Westmacott and U. Dahmen

Zeits. für Metallk. *(in press)*

The shape distribution of Ge precipitates in a quenched and aged Al-1.8% Ge alloy was characterized by transmission electron microscopy. In agreement with previous investigations, at least six different precipitate morphologies were distinguished: tetrahedra, octahedra and triangular plates all with the cube-cube orientation relationship; as well as laths along <100> Al directions, laths along <110> Al directions, and plates on {100} Al planes, with three different orientation relationships, respectively. The distribution of precipitate shapes was found to depend strongly on the heat treatment schedule. After quenching to 0° C, samples aged at 200° C exhibited predominantly triangular plates and tetrahedra and were insensitive to pre-aging at room temperature. By comparison, samples aged at 250 and especially at 300 C contained mainly lath-shaped precipitates after short pre-aging times, but a sharply increasing fraction of tetrahedra, octahedra and triangular plates for longer pre-aging times. When the temperature of the quench bath was raised from 0 to 40° C, samples aged at 200° C remained unchanged whereas samples aged at 250 and 300° C retained only lath shaped precipitates. Quenching directly to the three aging temperatures changed the precipitate distribution to a coarse array of large {100} plates.

37263 ■ Structure of 90° Domain Walls in Ferroelectric Barium Titanate Ceramics

L. Normand, R. Kilaas, Y. Montardi and A. Thorel

04th European Ceram. Soc. *(in press)*

Ferroelectric domain walls in tetragonal ferroelectric barium titanate ceramics are studied by means of electron microscopy. SEM and TEM observations are consistent with domain configuration already proposed. Conventional TEM measurements on SADP agree well with twin-related model currently admitted for ferroelectric domains. In spite of the very small lattice parameter variation during cooling (involving a small spontaneous strain) of BaTiO3 ceramics, displacements of specific features associated with atomic column positions are measured across domain walls on high resolution images. Using a dedicated image analysis software, these displacements are calculated with a high precision. 2D vector maps o the atomic displacements show different kinds of atomistic structure for different domain walls.

no # ■ **Transmission Electron Microscopy of Carbons for Lithium Intercalation**

K. Kinoshita, J. Bonevich, X. Song and T-D. Tran

10th Int'l Solid State Ionics *(submitted)*

Transmission electron microscopy (TEM) is a powerful tool which we are applying to study the microstructure of carbonaceous materials that are used as lithium-intercalation electrodes in lithium-ion cells. The results of our study on the relationship between the physiochemical properties of carbon, with strong emphasis on the microstructure observed by TEM, and their capability for electrochemical intercalation of lithium will be summarized. In addition, progress on the fabrication of a microcell for *in situ* TEM of lithium-intercalation in carbon will be discussed.

37086 ■ **Dynamic Observation of Electrochemical Etching in Silicon**

F.M. Ross and P.C. Searson

9th Int'l Micros. Semicon. Mats. *(in press)*

We have designed and constructed a TEM specimen holder in order to observe the process of pore formation in silicon. The holder incorporates electrical feedthroughs and a sealed reservoir for the electrolyte and accepts lithographically patterned silicon specimens. We describe the system and present preliminary, ex situ observations of the etching process.

no # ■ **Microstructural Evaluation of Deformation Mechanisms in Silicon Nitride Ceramics**

J.A. Schneider and A.K. Mukherjee

Am. Ceram. Soc. Conf. Proc. *(in press)*

Changes of phase composition and chemistry during deformation testing in compression of silicon nitride were investigated. The specimens were rapidly consolidated to maintain the initial alpha phase. In initial compressive deformation testing, 70% true strain was achieved at strain rates of 5×10^{-6} s^{-1}. Phase transformation was noted to occur during compressive deformation testing over the range of temperatures investigated. Grain boundary chemistry was determined with a JEOL 200 CX Analytical Electron Microscope (AEM) and an 8000 KEVEX System. The phase compositions of individual silicon nitride grains were determined by indexing of electron beam diffraction patterns.

38303 ■ **Microscopy Memories**

K.H. Westmacott

British Institute of Materials *(in press)*

This paper, to be published in "Towards the Millenium: A Materials Perspective," was presented at a meeting in Birmingham University commemorating Professor R.E. Smallman's 65th Anniversary. It traces some aspects of the authors' experiences in transmission electron microscopy over a 40-year span with particular emphasis on the value of collaborative research. The micrographs illustrate the advances that have been made over this period.

no # ■ **Special Crystalline Defects: Ferroelectric Domain Walls in $BaTiO_3$**

L. Normand, R. Kilaas, Y. Montardi and A. Thorel

Proc. GFC'95 *(in press)*

Paper written in French.

no # ■ **Telepresence for *In Situ* Electron Microscopy**

B. Parvin, J. Taylor, B. Crowley, L. Wu, W. Johnston, D. Owen, M.A. O'Keefe and U. Dahmen

Proc. IEEE Conference *(in press)*

We have developed a multimedia system for remote operation of scientific instruments that are designed for *in situ* microscopy. *In situ* experiments require dynamic adjustment of microscope controls as the specimen under observation is subjected to external stimuli such as temperature variation, straining, or gaseous environment. Control operation requires adjustments of external stimuli, adjustment of specimen position and orientation, and manipulation of microscope illumination, magnification, and focus. Normally a local operator makes such adjustments in response to the video signal from the microscope, but current wide area networks do not offer the real-time delivery guarantees that are required for the finely tuned adjustments requisite for dynamic studies. We have designed a system that eliminates the real-time delivery requirement. Using advanced computer vision algorithms locally, we have implemented drift correction (often severe during high-temperature experiments), automatic compensation of specimen movement during tilting, and automatic focus. The system has been used with a Kratos-1500 high-voltage transmission electron microscope, to make this unique facility — the highest voltage microscope in the United States — more widely available to users of the NCEM.

36543 ■ HREM Characterization of Invariant Line Interfaces and Structural Ledges in Mo-Si Alloys

S.Q. Xiao, U. Dahmen, S.A. Maloy and A.H. Heuer

Proc. iib'95 Mat. Sci. Forum *(in press)*

Two distinctly different morphologies of Mo_5Si_3 precipitates have been observed in a $MoSi_2$ single crystal matrix. The difference between these two morphologies is analyzed in detail by high resolution electron microscopy and explained by both the invariant line and the structural ledge theory, which are shown to predict identical interfaces.

37985 ■ Study of the Structure of Ferroelectric Domain Walls in Barium Titanate Ceramics

L. Normand, R. Kilaas, Y. Montardi and A. Thorel

Proc. iib'95 Mat. Sci. Forum *(in press)*

Barium titanate is a favorable material for theoretical study of ferroelectricity; small amounts of dopants can change drastically its properties, its crystallographic structure is relatively simple and reasonably stable under the beam in the Transmission Electron Microscope. Therefore, a thorough TEM study of various doped barium titanates may lead to fundamental insights of the elementary mechanisms of the ferroelectricity. In a first step, High Resolution Transmission Electron Microscopy images have been recorded. A computerized method has been developed to detect, measure and map the field of atomistic displacements on the images in comparison with a perfect lattice created from a non-distorted region of the image. In each case there is a displacement associated with the wall over a few unit cells which can easily be measured. Several examples will be given.

37619 **TEM Characterization of Invariant Line Interfaces and Structural Ledges in Mo-Si Alloy**

S.Q. Xiao, U. Dahmen, S.A. Maloy and A.H. Heuer

Proc. iib'95 Mat. Sci. Forum *(in press)*

Two distinct <110> lath morphologies of Mo_5Si_3 precipitates observed in $MoSi_2$ differ in their cross-sectional shape and lattice orientation. Type I laths exhibit a rectangular cross section, with interfaces parallel to low-index planes, while type II laths are parallelogram-shaped, with their major interface at 13° to the type I precipitate. The corresponding orientation relationships differ by a 1.8° rotation around the lath axis. In this study, the difference between the two characteristic morphologies and orientation relationships is shown to be the formation of an invariant line strain for type II precipitates. On an atomic scale, both interfaces have a terrace and ledge structure but differ in the stacking sequence of interfacial ledges associated with partial dislocations. The structural unit model and the invariant line model predict identical interface geometries which agree closely with the observations.

37912 **Misfit Dislocations Associated with Ultrathin Twins Along a Ni_3Al/Ni_3Nb Interface**

R. Bonnet, M. Loubradou, U. Dahmen and S. Hinderberger

Proc. iib'95 Mat. Sci. Forum *(in press)*

Typical defects of a Ni_3Al ($L1_2$)/Ni_3Nb (Do_a) faceted interface associated with the orientation relationships (11-1) Ni_3Al // (010)Ni_3Nb and [1-10] Ni_3Al // [100]Ni_3Nb are reported. High resolution electron microscopy reveals the presence, along the same interface, of ledges separating facets with different atomic structures. Some facets are associated with certain interfacial thicknesses since their structures involve one planar fault or an intermediate ultrathin Ni_3Al crystal. The observed ledges are associated with a misfit dislocation (MD) with $\mathbf{b}$ = (-1/6)[113]Ni_3Al. This vector is determined from the comparison of the experimental and simulated images. The multislice method has been applied with atom boxes which account for the elastic field surrounding each misfit dislocation core.

36909 ■ Size, Shape and Crystallinity of Luminescent Structures in Oxidized Si Nanoclusters and H-Passivated Porous Si

S. Schuppler, S.L. Friedman, M.A. Marcus, D.L. Adler, Y.-H. Xie, F.M. Ross, et al.

Proc. MRS 358 407 *1995*

Near edge and extended x-ray absorption fine structure measurements from a wide variety of H-passivated porous Si samples and oxidized Si nanocrystals, combined with electron microscopy, ir-absorption, α-recoil, and luminescence emission data, provide a consistent structural picture of the species responsible for the luminescence observed in these systems. For luminescent porous Si samples peaking in the visible region, i.e., <700nm, their mass-weighted-average structures are determined here to be particles - not wires, whose short-range character is crystalline - not amorphous, and whose dimensions - typically <15 Å - are significantly smaller than previously reported or proposed. These results depend only on sample luminescence behavior, not on sample preparation details, and thus have general implications in describing the mechanism responsible for visible luminescence in porous silicon. New results are also presented which demonstrate that the observed luminescence is unrelated to either the photo-oxidized Si species in porous Si or the interfacial suboxide species in the Si nanocrystals.

36911 ■ X-Ray Absorption Spectroscopy from H-Passivated Porous Si and Oxidized Si Nanocrystals

S. Schuppler, S. Friedman, M. Marcus, D. Adler, Y. Xie, F. Ross, et al.

Proc. MRS 375 113 *1995*

Quantum confinement in nanoscale Si structures is widely believed to be responsible for the visible luminescence observed from anodically etched porous silicon (por-Si), but little is known about the actual size or shape of these structures. EXAFS data from a wide variety of por-Si samples show significantly reduced average Si coordination numbers due to the sizeable contribution of surface-coordinated H. (The H/Si ratios, as large as 1.2, were independently confirmed by ir-absorption and α-recoil measurements). The Si coordinations imply very large surface/volume ratios, enabling the average Si structures to be identified as crystalline particles (not wires) whose dimensions are typically <15Å. Comparison of the Size-dependent peak luminescence energies with those of oxidized Si nanocrystals, whose shapes are known, shows remarkable agreement. Furthermore, NEXAFS measurements of the nanocrystals shows the outer oxide and interfacial suboxide layers to be constant over a wide range of nanocrystal sizes. The combination of these results effectively rules out surface species as being responsible for the observed visible luminescence in por-Si, and strongly supports quantum confinement as the dominant mechanism occurring in Si particles which are substantially smaller than previously reported or proposed.

37122 ■ **Simulation of Multicomponent Thin Film Deposition and Growth**

C.P. Burmester, L.T. Wille and R. Gronsky

Proc. MRS 389 59 *1995*

Results from a multicomponent Monte Carlo simulation of the deposition and growth of $YBa_2Cu_3O_7$ are presented and discussed. In particular, a detailed examination of the growth modes active during different morphological growth conditions is performed. At higher deposition rates, both [001] and [100] epitaxial variants ('c' and 'a' type growth, respectively) are observed to grow by modes attributed to the classic Volmer-Weber mechanism. At very low deposition rates, the film is observed to grow in a distinct, cyclic, multi-stage process. Small islands of [001] epitaxy nucleate and grow to one unit cell height followed by primarily horizontal growth or "ledge extension" until one unit cell layer has formed. This process then repeats. Simulated RHEED amplitude data from this growth process compares favorably to experimentally obtained data.

no # ■ **Relation Between Structure and Carrier Lifetime in As Implanted GaAs**

Z. Liliental-Weber, W. Swider, H. Kagiighi, A. Claverie, H.H. Wang and J.F. Whitaker

Proc. MRS 378 677 *1995*

The structure of As implanted GaAs layers before and after annealing are described and the relation between the structural quality and carrier lifetime was determined. Subpicosecond carrier lifetimes were found already for as-implanted layers, and this value changes only slightly after annealing in the temperature range up to 600°C. Annealing of As-implanted layers leads to the growth of As precipitates with a similar orientation relationship as those observed in low-temperature MBE-grown GaAs layers. However, it is still not clear whether point defects created by implantation or the As precipitates are responsible for the short carrier lifetime.

37394 ■ **Epitaxy and Magnetotransport Properties of $La_{0.8}Sr_{0.2}MnO_3$ Films Synthesized by Both Pulsed Laser Deposition and Novel Chemical Routes**

A.R. Modak and K.M. Krishnan

Proc. MRS *(in press)*

$La_{0.8}Sr_{0.2}MnO_3$ thin films with different microstructural characteristics were prepared by both pulsed laser deposition and a novel polymeric sol-gel process. For both techniques, polycrystalline films were obtained on Si(100) with a native oxide surface but epitaxial and highly oriented growth could be induced on lattice-matched $LaAlO_3$(100) substrates. While the overall magnetization and magnetoresistance behavior as a function of temperature and applied field were consistent with recent results, i.e., a semiconductor-to-metal transition accompanied by an antiferromagnetic- to-ferromagnetic transformation and large magnetoresistance at the resistance peak temperature, the properties of the films were significantly different depending on the microstructure, epitaxy and polycrystallinity. Detailed microstructural characterization of the films are presented and correlated with their magnetic/magnetotransport properties.

38159 ■ **Structural Defects in Heteroepitaxial and Homoepitaxial GaN**

Z. Liliental-Weber, S. Ruvimov, C. Kisielowski, Y. Chen, W. Swider, J. Washburn, N. Newman, A. Gassmann, X. Liu and L. Schloss, et al.

Proc. MRS *(in press)*

The microstructure and characteristic defects of heteroepitaxial GaN films grown on sapphire using MBE and MOCVD methods and of homoepitaxial GaN grown on bulk substrates are characterized by TEM, x-ray diffraction, and cathodoluminescence. The difference in arrangement of dislocations along grain boundaries and the influence of buffer layers on the quality of epitaxial films is described. The structural quality of GaN epilayers is compared to that of bulk GaN crystals grown from dilute solution of atomic nitrogen in liquid gallium. Homoepitaxial films grown using MOCVD showed the best quality and were almost free from extended defects. For the bulk GaN crystals a substantial difference in crystal perfection was observed near opposite c-faces of the plates. On one side the surface was almost atomically flat, and the underlying material was free of any extended structural defects, while the other side was rough, with a high density of planar defects. This difference was related to the polarity of the crystal. A large difference in crystal stoichiometry was also observed within different sublayers of the crystals. Based on convergent beam electron diffraction and cathodoluminescence, it is proposed that GaN antisite defects are related to the yellow luminescence observed in these crystals.

no # ■ **TEM/HREM Structural Characterization of Directionally Solidified GaAs-CrAs Eutectic**

S. Ruvimov, Z. Liliental-Weber, W. Swider, J. Washburn and D.E. Holmes

Proc. MRS *(in press)* 398

Conventional and high resolution electron microscopy have been applied to characterize the microstructure of the CrAs-GaAs eutectic. The CrAs-GaAs eutectic crystals were directionally solidified by the Czochralski method in order to produce an ordered array of CrAs rods embedded in a GaAs matrix. The CrAs rods of 2-3 μm in diameter align parallel to the growth axis of the ingot. Where the GaAs matrix is found to contain structural defects, the CrAs rods are effectively defect-free. The CrAs has an orthorombic structure with the parameters a=3.5±0.1 Å, b=6.2±0.1 Å, c=5.7±0.1Å. The c-axis is close to the direction of solidification.

37580 ■ **In Situ Observation of an Electrochemical Etching Reaction in Silicon**

F.M. Ross and P.C. Searson

Proc. MRS *(submitted)*

We are attempting to observe the kinetics of an electrochemical etching process by allowing the reaction to occur in real time within the electron microscope. We have designed and constructed a specimen holder for a JEOL 200CX microscope featuring a sealed reservoir which can be filled with an electrolyte. By observing the dynamics of the process, for example as a function of current density, we hope to understand the formation mechanism and to control the morphology of the pores produced. we will describe the progress of the experiments and present images showing the propagation of the etching front.

36955 ■ **HREM Structure Analysis of Σ13 Symmetrical Boundaries in Strontium Titanate Bicrystals**

J.E. Bonevich, S.Q. Xiao and U. Dahmen

Proc. MSA 53 568 *1995*

We have made detailed HREM observations of two Σ13 [001] tilt boundaries in strontium titanate, grown in the (320) and (510) symmetrical orientations, respectively. A rigid body translation has been found only for the (320) boundary which was shown to exhibit mirror glide symmetry. Both interfaces contained steps and pattern shifts consistent with the presence of DSC lattice dislocations. Cross correlation with a structural unit pattern template was applied as a useful technique to analyze the degree of similarity and precise location of characteristic motifs with the HREM images.

36956 ■ **High Resolution and Diffraction Contrast Imaging of Linear Islands Formed During Molecular Beam Epitaxy**

D. Loretto, F.M. Ross and C.A. Lucas

Proc. MSA 53 106 *1995*

There is currently a great deal of interest in the growth and properties of 'one-dimensional' structures. This is motivated by scientific curiosity and by the practical urge to fabricate faster, smaller and more efficient electronic and optical devices. It has recently been reported that under certain conditions linear islands can form spontaneously during growth. In this work we investigate linear CaF_2 islands which form on Si during molecular beam epitaxy. By combining low resolution diffraction contrast images from plan-view specimens with high resolution images from cross-section specimens, we determine that these islands are extremely uniform in width, can be as narrow as 5 nm, and extend over many 10s of μm. We postulate a mechanism for the formation of these novel features based on surface energy minimization.

36960 ■ In Situ Microscopy of the Anodic Etching of Silicon

F.M. Ross and P.C. Searson

Proc. MSA 53 232 *1995*

Porous semiconductors represent a relatively new class of materials formed by the selective etching of a single or polycrystalline substrate. Although porous silicon has received considerable attention due to its novel optical properties, porous layers can be formed in other semiconductors such as GaAs and GaP. We are attempting to gain a better understanding of the formation mechanism of porous silicon by allowing pore formation to occur in real time within the electron microscope. We have designed and constructed a specimen holder for a JEOL 200CX featuring a sealed reservoir which can be filled with an electrolyte such as HF. We have carried out ex situ experiments in which the application of 2-3V results in a total current of the order of 0.01 mA and pore growth at 10-100 nm s^{-1}.

36959 ■ Fresnel Effect in High Resolution TEM Imaging of Small Particles

V. Radmilovic and M.A. O'Keefe

Proc. MSA 53 564-65 *1995*

It is established that analysis of Fresnel contrast visible at the edges of nanoparticles in the high resolution electron microscope provides a valuable tool for determining the size of the particles with near-atomic-spacing accuracy. We have used HRTEM image simulation to explore the changes in images of a nanoparticle under various imaging conditions, in particular to relate the model particle size and its apparent size as derived from the HRTEM image. The minimal difference between particle and apparent sizes is obtained at a defocus approximately 400Å below the Gaussian image plane, i.e. close to the Scherzer value for the JEOL ARM 1000 of $\sqrt{(C_s\lambda)}$ = 448Å. At nearly all defocus settings above and below the Scherzer defocus, the spot intensity distribution does not correspond to the positions of the atoms in the particle, especially near a thick edge, leading to an apparent "relaxation" of atom positions near the particle edge. We believe that this effect is due to a strong Fresnel influence on the image, since the deviations between atoms and dots are more pronounced in regions close to the thick edges of small particles, i.e. in regions where the potential drop is sharper. For particles with both thick and tapering edges, this non-uniform apparent "relaxation" may even change the aspect ratio of the image so that the particle appears "taller" or "wider" in the electron micrograph.

36965 Automated Measurement of Size and Visibility of Small Inclusions in HREM Images

S. Paciornik, S.-Q. Xiao, S. Hinderberger, E. Johnson and U. Dahmen

Proc. MSA 53 648 *1995*

This work describes an automatic image analysis method for measuring the visibility and apparent size of inclusions in a matrix, imaged by HREM. The method is based on intensity changes between the matrix and inclusion regions of the image. It provides a quantitative way of describing changes that are generally interpreted only in a qualitative sense. It also allows for measurements in situations of very low visibility where visual estimates are nearly impossible. The method measures the mean squared intensity difference between lines of an image defined as: $R = \text{mean}[I_m(\mathbf{x}) - I_m(\mathbf{x}_0)^2]$. $I_m(\mathbf{x})$ is a line, selected by the user, which is scanned across the image. $I_m(\mathbf{x}_0)$ is the first line of the scan, taken in a region away from the inclusion. For each position of $I_m(\mathbf{x})$, $I_m(\mathbf{x}_0)$ is subtracted pixel by pixel, and the average of all squared intensity differences, is obtained (R).

36966 ■ Modeling and Simulation of Octahedral Pb Inclusions in Al

S.-Q. Xiao, S. Paciornik, R. Kilaas, E. Johnson and U. Dahmen

Proc. MSA 53 646 *1995*

This work describes the modeling and image simulation of octahedral Pb inclusions in Al. A variety of supercells was built, containing Pb inclusions of 2,3,4 and 5 moiré spacings in size, each in a matrix with 5 total thicknesses from ~0.5 to ~1.5 Al extinction distances (ξAl = 24 nm at 800 kV), and at three different depths for each size and each thickness. The largest supercells included ~70000 atoms. Each supercell was composed of a number of thin slabs with plane normal parallel to <110>. Using CrystalKit, each slab was built to contain an AB stacking of Al atoms (2.86Å thick), the smallest repeat distance along <110> in Al. While the Al lattice repeats in each slab, the Pb lattice does not, due to the lattice mismatch between the two lattices and this was considered in creating subsequent slabs. Finally, the supercell was built by stacking all the slabs together thus creating 4 edge-on and 4 inclined interfaces. Atomic relaxation at the interfaces was not considered in these models. In order to test the visibility of steps at the interfaces, supercells containing an atomic ledge in one of the {111} interfaces were also built. Using NCEMSS running on a DEC Alpha station, image simulations were carried out for 9 defoci ranging from -30 nm to -110 nm.

36967 ■ **Refinement of Rigid Shift Component Normal to a Σ5 Grain Boundary in Rutile by Quantitative HREM**

S. Paciornik, D. Michel and U. Dahmen

Proc. MSA 53 570 *1995*

In the present work we describe a method for measurement of rigid shifts, that optimizes the fit between simulated and experimental images with respect to the magnitude of the rigid shift as a variable. The technique compares experimentally observed with modeled images using the normalized cross correlation coefficient as a measure for the goodness of fit. To avoid complications from elastic distortions, misorientations or extended relaxations, this optimization is applied only to a small segment of the image depicting a structural unit characteristic for the interface.

36968 ■ **The NCEM Public Domain Software Library of Extensions to Digital Micrograph**

R. Kilaas and S. Paciornik

Proc. MSA 53 628 *1995*

A number of image processing algorithms have been developed at the NCEM as part of the ongoing research at the center. These routines are being made public in an effort to serve the electron microscopy community and will be made available through the NCEM world wide web home page. The first routines to be released all run under the Digital Micrograph image processing software from Gatan, Inc. and include extensions for peak-finding, lattice fit, displacement analysis, template matching, unit averaging and reduction of noise due to amorphous surface contamination.

36969 ■ A Project for On-Line Remote Control of a High-Voltage TEM

B. Parvin, D. Agarwal, D. Owen, M.A. O'Keefe, K.H. Westmacott, U. Dahmen and R. Gronsky

Proc. MSA 53 82 *1995*

A project has recently been established to provide users of the NCEM with remote on-line access to a 1.5MeV Kratos EM-1500 high-voltage transmission electron microscope via existing wide area networks. Within this project we are developing and implementing a set of tools, protocols, and interfaces to bring transmission electron microscopy on-line for collaborative research. Initially applied to the Kratos, the project will provide increased utilization of this unique instrument with its heretofore restricted access due to its sensitive components and demand for sophisticated operator skills. Additionally, the project will provide computer tools for capturing and manipulating real-time audio and video signals. These tools will be integrated into a standardized user interface that may be used for remote access to any transmission electron microscope equipped with a suitable control computer. This work is a first step towards a new kind of availability for unique microscopes located at central facilities. It will allow collaborations where multiple people at remote locations can monitor the experiments and discuss results while it is in progress. It will provide much greater accessibility to the microscope, and the new methods of controlling the microscope will greatly ease the operators task, leaving them free to concentrate on the science rather than the mechanics of running the microscope.

36989 ■ Microstructural Evolution of γ-Alumina Supported Rhodium Catalysts

Z. Weng-Sieh, R. Gronsky and A.T. Bell

Proc. MSA 53 400 *1995*

In an era of increasing environmental awareneess, stricter federal and state regulation of pollutant emissions are emerging. A major source of pollution arises from automobiles which inadvertently form gaseous products such as nitric oxide, carbon monoxide, and hydrocarbons. Since the early 1980's these effluents have been converted to safer forms using a three-way catalytic converter that employs a high dispersion of rhodium and platinum particles supported on a large surface area of transitional γ-phase alumina. Unfortunately, such a converter is susceptible to decreased performance over time, and this degredation has been attributed to changes in the catalyst microstructure. The nanoscaled nature of the transition metal catalysts and the submicron-scaled size of the transitional alumina necessitates the use of the high spatial resolution analyses made possible by transmission electron microscopy.

37069 ■ Where are the Limits to Spatial Resolution in the HRTEM?

M.A. O'Keefe

Proc. MSA 53 280 *1995*

The spatial resolution of a HRTEM is an upper bound on the resolution of images that can be produced by that microscope, with no guarantee that any particular image from the microscope will attain this bound. In addition to instrumental limits, specimen properties will degrade image resolutions. For small-cell crystalline specimens, allowable resolutions will be quantized to the Bragg reflections. "Resolution" has traditionally been defined in terms of the microscope's Scherzer resolution limit at optimum defocus. However, even beyond the Scherzer limit, it is possible to transfer spatial frequencies from the specimen to the image, out to the information limit of the electron microscope. By successively tuning the HRTEM to pass different spatial frequency bands by choosing suitable defocus settings, then combining these images into one, we obtain a resolution that approaches the information limit of the microscope. With this technique a microscope's resolution will no longer be determined by its Scherzer limit, but will become identical to its information limit.

37070 ■ Advances in Image Simulation for High Resolution TEM

M.A. O'Keefe

Proc. MSA 53 38 *1995*

Advances in image simulation have occurred on several fronts since mainstream application of image simulation to routine structure determination by HRTEM was ushered in by the SHRLI programs. There has been steady improvement in modeling algorithms, including aberrations such as three-fold astigmatism. The most important advance is quantitative matching of simulated with experimental images. The experimental image is digitized, compared with simulations, and a "goodness-of-fit" parameter computed. For periodic specimens, comparison can be carried out in real space, comparing intensities of the images pixel by pixel, or in reciprocal space comparing the image intensity spectra. The process can be automated and the simulation fit improved to yield the best matching image from a given model crystal structure. An automated two-step process can be used for refinement of an unknown structure, in the case where an experimental image is available with an unknown structure close to a known one. King and Campbell used an automated non-linear least-squares image-matching process to establish image parameters and refine the structure of a grain boundary, allowing the program to vary atom positions to achieve the best match and produce a refined structure model. Möbus and Rühle used a Gauss-Seidel bivariant search method to refine the structure of a niobium-sapphire interface.

37036 ■ Chemical Sensitivity of Convergent Beam Electron Diffraction on the Stoichiometry of GaN

Z. Liliental-Weber, C. Kisielowski and J. Washburn

Proc. MSA 53 148 *1995*

III-V nitride thin film growth has attracted considerable attention because it now seems feasible to engineer semiconductor band gaps between 2.1 and 6.2 eV. One of the challenges coming with this development is related to the fact that structural perfection seems not to correlate directly with optical properties such as the emission of blue-green or UV light in GaN. In order to better understand this material, high resolution transmission electron microscopy (HREM) and convergent beam electron diffraction (CBED) experiments were used to study structural defects in GaN thin films. Experiments were performed with a Topcon 002B and ARM operating at 200 and 800 KeV, respectively, and were guided by image simulations.

37233 ■ Techniques for In Situ HVEM Mechanical Deformation of Nanostructured Materials

M.A. Wall, T.W. Barber Jr. and U. Dahmen

Proc. MSA 53 240 *1995*

We have developed two *in situ* HVEM experimental techniques which allow us to begin fundamental investigations into the mechanisms of deformation and fracture in nanostructured materials. First, a procedure for the observation of tensile deformation and failure of multilayer (ML) materials in cross-section is detailed. Second, the development of an *in situ* HVEM nanoindentor of surfaces and films on surfaces in cross-section is presented.

37360 ■ **Superconductivity and Observation of Ordered Structures in Deintercalated Li_xNbO_2**

M. Fendorf, M.A. Rzeznik and A.M. Stacy

Proc. MSA 53 376 *1995*

We have observed the appearance of extra reflections in [001] diffraction patterns obtained from deintercalated Li_xNbO_2 materials, primarily a tripling along <110> and a doubling along <100>, and find the corresponding periodicities in high-resolution images. The occurrence of extra reflections in these diffraction patterns can be explained either by the presence of charge density waves in Li_xNbO_2, or by ordering of Li-vacancies after deintercalation. However, charge density waves are not expected to be stable in solids at room temperature, and we did not observe the development of any additional periodicities in a sample cooled to 100K. We thus attribute our images and diffraction patterns to the ordering of vacancies created as Li is removed from the host structure. The ordering of Li, apparently with two preferred periodicities, may be related to a phase separation revealed by magnetic measurement.

---

no # ■ **Lorentz Microscopy Observation of Vortex Dynamics Due to Transport Current**

T. Yoshida, H. Kasai, J.E. Bonevich, T. Matsuda and A. Tonomura

Proc. MSA 53 366 *1995*

At present, Lorentz microscopy is the only method to visualize individual vortices in superconductors and observe their motion in real time. Using this technique, we have investigated the fascinating vortex dynamics in superconductors, niobium and BSCCO, and recently applied it to investigate current driven vortex motion.

no # ■ **Dynamical Lorentz TEM Observation of Exchange Coupling in MR $Ni_{0.80}Fe_{0.20}$/NiO Films**

W. Cao

Proc. MSA 53 110 *1995*

In our research program involved with materials showing magnetoresistive (MR) phenomena, attention has been given to detailed microstructural analyses in order to understand physical properties and other characteristics. One of the biggest problems in the MR sensor application is the noise associated with Barkhausen jumps due to magnetic domain wall motion in the MR sensor, usually permalloy films ($Ni_{0.80}Fe_{0.20}$). It has been found that when a permalloy film was deposited together with an antiferromagnetic film such as FeMn, the noise could be suppressed. It is known that there is an exchange coupling field (He) in the $Ni_{0.80}Fe_{0.20}$/FeMn bilayers through the interface, and it is this exchange coupling field that makes the MR sensor a single domain which suppresses the noise. However, FeMn antiferromagnetic fiims have poor corrosion resistance, and this provides a motivation to find a substitute material for FeMn. Lorentz imaging is a useful method for understanding ferro- and antiferromagnetic coupling in complex multilayers.

no # ■ **Microstructure and Microanalysis of Neodymium Iron Boron Magnets Sintered with Aluminum**

M. Chandramouli and G. Thomas

Proc. MSA 53 486 *1995*

The magnetic properties of NdFeB magnets sintered with 15 vol.% Al at 850° C and 1000° C for one hour are dependent on microstructure. Complementary use of SEM and TEM techniques are crucial to elucidate the microstructural differences responsible for the properties. The hysteresis loops shown indicate that the higher sintering temperature sample has a larger dip near zero applied field and lower coercivity. This behavior is consistent with a larger volume of soft magnetic phases.

38298 ■ High Energy As Ion Implantation to GaAs

J. Jasinski, Z. Liliental-Weber, M. Kaminska, J. Washburn and C. Jagadish

Proc. MSA 53 458 *1995*

Over the last few years there have been many studies of GaAs layers grown in the temperature range from 180° C to 300° called LT-GaAs. These studies were motivated by the potential applications of that material in microwave and fast optoelectronic devices. Annealed LT-GaAs layers have interesting electrical properties, including high resistivity and short photocarrier lifetime connected with the nonstoichiometry of that material. However, it is still not clear whether arsenic antisite point defects or arsenic precipitates formed during annealing cause these interesting properties of LT GaAs. This paper reports the first results of TEM investigations on GaAs implanted with high energy arsenic ions.

no # ■ Structure and Device Characteristics of $SrBi_2Ta_2O_9$ Memories

J.F. Scott, F.M. Ross, C.A. Paz de Araujo, M.C. Scott and M. Huffman

MRS Bulletin *1996*

Electron micrographs of the layer-structure perovskites ($SrBi_2Ta_2O_9$) that have become the materials of choice for non-volatile computer memories [Paz de Araujo et al., Nature 374, (1995) p. 627] reveal very complicated structures. In bulk form this family of materials exists primarily in a structure with two TaO_6 octahedra interrupted by Bi_2O_2 planes. The thin-film forms are complicated, with amorphous regions and second phases. Mechanisms of leakage current and electrical breakdown in these materials are discussed.

NOTES

NOTES

NOTES

National Center for Electron Microscopy
Berkeley Lab
MS 72
Berkeley, CA 94720
U.S.A.

National Center for Electron Microscopy
Berkeley Lab
MS 72
Berkeley, CA 94720
U.S.A.

Please send a reprint of the paper(s):

Number	First Author	Title (first two words)

Name_____ Date_____

Affiliation _____

Address _____

_____

Please send a reprint of the paper(s):

Number	First Author	Title (first two words)

Name_____ Date_____

Affiliation _____

Address _____

_____

☆ U.S. Government Printing Office: 1991 587-703

National Center for Electron Microscopy
Ernest Orlando Lawrence
Berkeley National Laboratory
University of California
Berkeley, CA 94720